Prepared for submission to JHEP

Dynamical holographic QCD model for glueball and light meson spectra

Danning Li [a], **Mei Huang**[a,b]
[a] **Institute of High Energy Physics, Chinese Academy of Sciences, Beijing, China**
[b] **Theoretical Physics Center for Science Facilities, Chinese Academy of Sciences, Beijing, China**

Abstract: In this work, we offer a systematic framework to describe the gluodynamics and chiral dynamics. We firstly construct a quenched dynamical holographic QCD (hQCD) model in the graviton-dilaton framework for the pure gluon system, then develop a dynamical hQCD model for the two flavor system in the graviton-dilaton-scalar framework by adding light flavors on the gluodynamical background. The dimension-2 dilaton background field Φ takes the same form as that in the soft-wall model and its square Φ^2 can be identified as the dual field to the gauge invariant operator of the dimension-4 gluon condensate. The gluon condensate in the QCD vacuum breaks conformality and induces a deformed warp factor. Without introducing extra parameters but just self-consistently solving the deformed metric induced by the dilaton background field, we find that the scalar glueball spectra in the quenched dynamical model is in very well agreement with lattice data. For two flavor system in the graviton-dilaton-scalar framework, the deformed metric is self-consistently solved by considering both the chiral condensate and gluon condensate in the vacuum, which are responsible for the chiral symmetry breaking and linear confinement, respectively. It is found that the mixing between the chiral condensate and gluon condensate is important to produce the correct light flavor meson spectra. The pion form factor and the vector couplings are also investigated in the dynamical hQCD model. Besides, we give the criteria for the existence of linear quark potential from the metric structure, and show a negative quadratic dilaton background field is not favored in the graviton-dilaton framework.

Keywords: Graviton-dilaton-scalar system, gluon condensate, linear confinement, chiral condensate, chiral symmetry breaking

Contents

1 Introduction

The local quantum field theoretical description has made great success since it was firstly developed in the quantization of electrodynamics and further been developed and applied to the descriptions of elementary particles. Nowadays, quantum chromodynamics (QCD) is accepted as the fundamental theory of the strong interaction. In the ultraviolet (UV) or weak coupling regime of QCD, the perturbative calculations agree well with experiment.

However, in the infrared (IR) regime, the description of QCD vacuum as well as hadron properties and processes in terms of quark and gluon still remains as outstanding challenge in the formulation of QCD as a local quantum field theory. In order to derive the low-energy hadron physics and understand the deep-infrared sector of QCD from first principle, various non-perturbative methods have been employed, in particular lattice QCD [1–4], Dyson-Schwinger equations (DSEs)[5, 6], and functional renormalization group equations (FRGs)[7–9].

In recent decades, an entirely new method based on the anti-de Sitter/conformal field theory (AdS/CFT) correspondence and the conjecture of the gravity/gauge duality [10–12] provides a revolutionary method to tackle the problem of strongly coupled gauge theories. Though the original discovery of holographic duality requires supersymmetry and conformality, the holographic duality has been widely used in investigating hadron physics, strongly coupled quark gluon plasma and condensed matter. It is widely believed that the duality between the quantum field theory and quantum gravity is an unproven but true fact. In general, holography relates quantum field theory (QFT) in d-dimensions to quantum gravity in (d + 1)-dimensions, with the gravitational description becoming classical when the QFT is strongly-coupled. The extra dimension can be interpreted as an energy scale or renormalization group (RG) flow in the QFT [13–20].

Many efforts have been invested in applying holography duality to describe the real QCD world, e.g. for mesons [21–23], baryons [24] and glueballs [25], see Refs. [26, 27] for reviews. It is well-known that the QCD vacuum is characterized by spontaneous chiral symmetry breaking and color charge confinement. The chiral symmetry breaking can be read from the mass difference between the chiral partners of the hadron spectra, and the spontaneous chiral symmetry breaking is well understood by the dimension-3 quark condensate $\langle\bar{q}q\rangle$ [28] in the vacuum. The understanding of confinement remains a challenge [29]. From the hadron spectra, confinement can be read from the Regge trajectories of hadrons [30, 31], which suggests that the color charge can form the string-like structure inside hadrons. Confinement can also manifest itself by the linear potential between two quarks at large distances [32].

A successful holographic QCD model should describe chiral symmetry breaking, and at the same time should describe both the Regge trajectories of hadron spectra and linear quark potential, two aspects in the manifestation of color confinement. Nonetheless, these important nonperturbative features haven't been successfully accommodated in a unique hQCD model.

The current achievements of AdS/QCD models for hadron spectra are the hard-wall AdS/QCD model [21] and the soft-wall AdS/QCD or KKSS model [22]. In the hard-wall model [22], the chiral symmetry breaking can be realized by chiral condensation in the vacuum, however, the resulting mass spectra for the excited mesons behave as $m_n^2 \sim n^2$, which is different from the linear Regge behavior $m_n^2 \sim n$. In order to generate the linear Regge behavior, the authors of Ref.[22] introduced a quadratic dilaton background, one can obtain the desired mass spectra for the excited vector mesons, while the chiral symmetry breaking phenomenon cannot be consistently realized [33].

Interesting progress was made in Refs. [34, 35], where a quartic interaction term in the

bulk scalar potential was introduced to incorporate linear trajectories and chiral symmetry breaking. However, such a term was shown [35] to result in a negative mass square for the lowest lying scalar meson state, which might cause an instability of the background. In Ref.[36], a deformed warp factor is introduced, which can cure the instability and maintain the linear behavior of the spectra.

With AdS_5 metric in the soft-wall model and its extended versions [34–41] (except [36]), only Coulomb potential between the two quarks can be produced [42]. On the other hand, the linear quark potential can be realized in the Andreev-Zakharov model [43], where a positive quadratic correction in the deformed warp factor of AdS_5 geometry was introduced. The linear heavy quark potential can also be obtained by introducing other deformed warp factors as in Refs. [44, 45]. The positive quadratic correction in the deformed warp factor in some sense behaves as a negative dilaton background in the 5D action, which motivates the proposal of the negative dilaton soft-wall model [46, 47]. More discussions on the sign of the dilaton correction can be found in [48, 49].

It is noticed that the quadratic correction, whether appears in the 5D action or in the deformed warp factor, indeed plays an important role to realize the linear confinement, though only partly. Since both the Regge trajectories of hadron spectra and linear quark potential are two aspects in the manifestation of color confinement, they should share the same dynamical origin and should be realized in the same holographic QCD model.

In the soft-wall model and its improved versions, the dilaton field or the deformed warp factor are introduced by hand. In Ref.[50], we have successfully described the chiral symmetry breaking, the Regge trajectories of hadron spectra and linear quark potential in the graviton-dilaton-scalar coupling framework, in which the metric, the field(s) and the potential(s) of the field(s) are self-consistently determined by field equations, and one can self-consistently solve out the other two with one input. There are at least three different ways to deal with the system in the literature: 1) Input the form of the field(s) to solve the metric structure and the potential(s) of the field(s) [50, 51]; 2) Input the potential(s) of the field(s) to solve the metric and the field(s) [52, 53]; 3) Input the form of the metric structure to solve the field(s) and the potential(s) of the field(s) [54].

This work is an extension of Ref.[50], and we intend to establish the relation between the QCD dynamics including at IR and its induced geometry. The paper is organized as follows: In Sec. 2, we establish a quenched dynamical hQCD model in the graviton-dilaton framework to describe the pure gluon system, and by selfconsistently solve the deformed warp factor induced by the dilaton field, we get the scalar glueball spectra; We introduce the meson spectra in the KKSS model and its improved versions in Sec.3; We then develop the graviton-dilaton-scalar coupling framework for two flavor system and investigate the hadron spectra in Sec.4, and we also investigate pion form factors and vector couplings in Sec. 5. We give discussion and summary in Sec.6.

2 Pure gluon system: quenched dynamical holographic model

At the classical level, QCD is a scale invariant theory, which is broken by quantum fluctuations. The pure gluon part of QCD Lagrangian in 4-dimension is described by

$$\mathscr{L}_G = -\frac{1}{4} G^a_{\mu\nu}(x) G^{\mu\nu,a}(x), \tag{2.1}$$

with

$$G^a_{\mu\nu}(x) = \partial_\mu A^a_\nu(x) - \partial_\nu A^a_\mu(x) + g f^{abc} A^b_\mu(x) A^c_\nu(x). \tag{2.2}$$

Where $A_\mu(x)$ is the gluon field with $a = 1, \cdots, 8$ the color indices.

In the vacuum, the scale invariance is explicitly broken, and the relevant degrees of freedom of QCD at infrared are still poorly understood. Varies of vacuum condensates provide important information to understand the non-perturbative dynamics of QCD. For example, the gauge invariant dimension-4 gluon condensate $\langle g^2 G^2 \rangle$ has been widely investigated in both QCD sum rules and lattice calculations [55–57], and the non-vanishing value of the condensate does not signal the breaking of any symmetry directly, but rather the non-perturbative dynamics of strongly interacting gluon fields. In last decade, there have been growing interests in dimension-2 gluon condensates $\langle g^2 A^2 \rangle$ in SU(N_c) gauge theory and its possible relation to confinement [58–74].

On the other hand, the effective Lagrangian for pure gluon system can also be constructed in terms of lightest glueball [75–77] or one scalar particle - dilaton [78–83]. The dilaton field is an hypothetical scalar particle predicted by string theory and Kaluza-Klein type theories, and its expectation value probes the strength of the gauge coupling. In Ref.[80], an effective coupling of a massive dilaton to the 4-dimensional gauge fields provides an interesting mechanism which accommodates both the Coulomb and confining potentials between heavy quarks. In the following, we construct a 5-dimension dynamical hQCD model in the graviton-dilaton coupled system for the pure gluodynamics.

2.1 Quenched dynamical holographic model and gluodynamics

Csaki and Reece in Ref.[51] proposed to model the pure gluon system in the graviton-dilaton framework by considering the correspondence between the dilaton background field and the non-perturbative gluon condensate, which provides a natural IR cut-off. They investigated the case of dilaton field coupling with dimension-4 gluon operator $\mathrm{Tr}\langle G^2 \rangle$ and higher dimension-6 gluon condensation $\mathrm{Tr}\langle G^3 \rangle$, and found that such IR correction cannot generate Regge spectra of glueball. They also discussed a tachyon-dilaton-graviton system, where the tachyon corresponds to a dimension-2 gluon condensate $\langle g^2 A^2 \rangle$ to realize the linear confinement. However, the local dimension-2 gluon operator is not gauge invariant.

We construct a 5D effective model for pure gluon system by introducing one scalar dilaton field $\Phi(z)$ in the bulk. It is not known how the dilaton field should couple with the gauge field in 4-dimension. Motivated by Refs.[77] and [80], we introduce the holography dictionary as $\Phi^2(z)$ dual to the gauge invariant dimension-4 gluon condensation $\mathrm{Tr}\langle G^2 \rangle$. In this case, though the dilaton field $\Phi(z)$ itself has dimension of 2, the action is always in terms of Φ^2 thus there is no gauge invariant problem.

The 5D graviton-dilaton coupled action in the string frame is given below:

$$S_G = \frac{1}{16\pi G_5}\int d^5x\sqrt{g_s}e^{-2\Phi}\left(R_s + 4\partial_M\Phi\partial^M\Phi - V_G^s(\Phi)\right). \tag{2.3}$$

Where G_5 is the 5D Newton constant, g_s, Φ and V_G^s are the 5D metric, the dilaton field and dilaton potential in the string frame, respectively. The metric ansatz is often chosen to be

$$g^s_{MN} = b_s^2(z)(dz^2 + \eta_{\mu\nu}dx^\mu dx^\nu), \quad b_s(z) \equiv e^{A_s(z)}. \tag{2.4}$$

In this paper, the capital letters like "M,N" would stand for all the coordinates(0,1,..,4), and the greek indexes would stand for the 4D coordinates(0,...,3). We would use the convention $\eta^{00} = \eta_{00} = -1, \eta^{ij} = \eta_{ij} = \delta_{ij}$.)

Under the frame transformation

$$g^E_{mn} = g^s_{mn}e^{-2\Phi/3}, \quad V_G^E = e^{4\Phi/3}V_G^s, \tag{2.5}$$

Eq.(2.3) becomes

$$S_G^E = \frac{1}{16\pi G_5}\int d^5x\sqrt{g_E}\left(R_E - \frac{4}{3}\partial_m\Phi\partial^m\Phi - V_G^E(\Phi)\right). \tag{2.6}$$

The equations of motion can be easily derived by doing functional variation with respective to the corresponding fields. It takes the familiar form in the Einstein frame,

$$E_{mn} + \frac{1}{2}g^E_{mn}\left(\frac{4}{3}\partial_l\Phi\partial^l\Phi + V_G^E(\Phi)\right) - \frac{4}{3}\partial_m\Phi\partial_n\Phi = 0, \tag{2.7}$$

and

$$\frac{8}{3\sqrt{g_E}}\partial_m(\sqrt{g_E}\partial^m\Phi) - \partial_\Phi V_G^E(\Phi) = 0. \tag{2.8}$$

The simplest dimension-2 dilaton background field has the quadratic form as

$$\Phi = \pm\mu_G^2 z^2. \tag{2.9}$$

The positive quadratic dilaton background is the same as the one introduced in the KKSS model [22]. We will show in Section 2.2 and 2.3 that only positive quadratic correction can generate the linear confinement.

Under the metric ansatz Eq.(2.4), the above Einstein equations has two independent equations,

$$-A_E^{''} + A_E^{'2} - \frac{4}{9}\Phi^{'2} = 0, \tag{2.10}$$

$$\Phi^{''} + 3A_E^{'}\Phi^{'} - \frac{3}{8}e^{2A_E}\partial_\Phi V_G^E(\Phi) = 0. \tag{2.11}$$

in the new variables of

$$b_E(z) = b_s(z)e^{-\frac{2}{3}\Phi(z)} = e^{A_E(z)}, \quad A_E(z) = A_s(z) - \frac{2}{3}\Phi(z). \tag{2.12}$$

In the string frame, the above two equations of motion become

$$-A_s^{''}-\frac{4}{3}\Phi^{'}A_s^{'}+A_s^2+\frac{2}{3}\Phi^{''}=0, \tag{2.13}$$

$$\Phi^{''}+(3A_s^{'}-2\Phi^{'})\Phi^{'}-\frac{3}{8}e^{2A_s-\frac{4}{3}\Phi}\partial_\Phi(e^{\frac{4}{3}\Phi}V_G^s(\Phi))=0. \tag{2.14}$$

With the quadratic dialton background given in Eq.(2.9), we can solve the metric A_E and the dilaton potential $V_G^E(\Phi)$ in the Einstein frame as

$$A_E(z)=\log(\frac{L}{z})-\log({}_0F_1(5/4,\frac{\Phi^2}{9})), \tag{2.15}$$

$$V_G^E(\Phi)=-\frac{12\,{}_0F_1(1/4,\frac{\Phi^2}{9})^2}{L^2}+\frac{16\,{}_0F_1(5/4,\frac{\Phi^2}{9})^2\Phi^2}{3L^2}, \tag{2.16}$$

with ${}_0F_1(a;z)$ the hypergeometric function. It is noticed that in the Einstein frame, both the positive and negative quadratic correction give the same results. However, in the string frame, the positive quadratic dilaton background field $\Phi^+=\mu_G^2z^2$ gives:

$$A_s^+=A_E(z)+\frac{2}{3}\mu_G^2z^2,\ V_G^{s,+}=e^{-4/3\mu_G^2z^2}V_G^E, \tag{2.17}$$

and the negative dilaton background field $\Phi^-=-\mu_G^2z^2$ gives

$$A_s^-=A_E(z)-\frac{2}{3}\mu_G^2z^2,\ V_G^{s,-}=e^{4/3\mu_G^2z^2}V_G^E. \tag{2.18}$$

We will show in Section 2.2 and 2.3 that positive and negative quadratic dilaton background will induce different results on the glueball spectra and the quark-antiquark potential.

With the normalized variable Φ_N which is defined as

$$\Phi\to\sqrt{\frac{3}{8}}\Phi,\quad -\frac{4}{3}\partial_M\Phi\partial^M\Phi\to-\frac{1}{2}\partial_M\Phi\partial^M\Phi, \tag{2.19}$$

the dilaton potential in the Einstein frame takes the form of

$$V_G^E(\Phi)=-12\,\frac{{}_0F_1(1/4;\frac{\Phi^2}{24})^2}{L^2}+2\,\frac{{}_0F_1(5/4;\frac{\Phi^2}{24})^2\Phi^2}{L^2}, \tag{2.20}$$

here L the radius of AdS_5 and ${}_0F_1(a;z)$ the hypergeometric function. In the ultraviolet limit,

$$V_G^E\overset{\Phi\to0}{\longrightarrow}-\frac{12}{L^2}+\frac{1}{2}M_\Phi^2\Phi^2, \tag{2.21}$$

with the 5D mass for the dilaton field

$$M_\Phi^2L^2=-4. \tag{2.22}$$

From the AdS/CFT dictionary $\Delta(\Delta-4)=M_\Phi^2L^2$, one can derive its dimension $\Delta=2$, which is consistent with our ansatz that Φ^2 corresponds to dimension-4 gluon condensate. It is worth to emphasize that even though the dilaton field itself has dimension of 2, however, because it always appears in the action in the form of Φ^2, there is no gauge invariant problem in our framework.

We call this 5D model for pure gluon system as the quenched dynamical soft-wall holographic model. The gluon content of the dimension-2 dilaton field itself is not clear to us yet, there are several possibilities:

n(0^{++})	Lat1	Lat2	Lat3	Lat4	Lat5
	$N_c = 3$	$N_c = 3$	$N_c \to \infty$	$N_c = 3$	$N_c = 3$
1	1475(30)(65)	1580(11)	1480(07)	1730(50)(80)	1710(50)(80)
2	2755(70)(120)	2750(35)	2830(22)	2670(180)(130)	
3	3370(100)(150)				
4	3990(210)(180)				

Table 1. Lattice data for 0^{++}*glueball* in unit of MeV. Lat1 data from Ref.[91], Lat2 and Lat3 data from Ref.[92], Lat4 [93] and Lat5 [94] are anisotropic results.

1. The dimension-2 dilaton might be dual to the dimension-2 gluon condensate $\langle g^2 A^2 \rangle$ [61, 64, 65], which has been discussed in some literatures, e.g. Refs.[35, 39, 43, 51]. However, it encounters the gauge invariant problem.

2. The simplest gauge invariant dimension-2 gluon operator is the zero momentum mode of $\langle g^2 A^2 \rangle$, i.e. $< g^2 A^2(k = 0) >$, the Bose-Einstein condensation (BEC) of the "pairing" of two gluons in the vacuum due to the strong interaction [58, 68]. The BEC of the "pairing" of two gluons spontaneously generates an effective gluon mass and breaks scale invariance, and in this scenario, the dimension-4 gluon condensation is proportional to the dimension-2 gluon condensation. Recent lattice results support a gluon mass at IR [84–86] which was proposed by Cornwall in 1981 [87] and recently developed in [88].

3. The dimension-2 dilaton field might also correspond to the gauge invariant but non-local operator related to topological defects in the QCD vacuum [64].

We leave the fundamental problem on the basic degree of freedom of QCD vacuum and the mechanism of confinement for further studies. In the following, we show that the results of glueball spectra and linear potential based on the simplest ansatz of dimension-2 dilaton background field in Eq.(2.9).

2.2 Scalar glueball spectrum in quenched dynamical holographic model

The glueball spectrum has attracted much attention more than three decades [89]. The study of particles like glueballs where the gauge field plays a more important dynamical role than that in the standard hadrons, offers a good opportunity of understanding the nonperturbative aspects of QCD, e.g. see reviews [90]. In Table 1, we list the scalar glueball spectra from several lattice groups [91–94].

The glueball has been studied in the holographic QCD models [95–98]. The scalar glueball $\mathscr{G}$ is associated with the local gauge-invariant QCD operator $tr(G_{\mu\nu}G^{\mu\nu})$ defined on the boundary spacetime, which has dimension $\Delta_{\mathscr{G}} = 4$. From the AdS/CFT dictionary, the scalar glueball has zero 5D mass, i.e. $M^2_{\mathscr{G},5} = 0$.

We assume the glueball can be excited from the QCD vacuum described by the quenched dynamical holographic model in Section 2.1, and the 5D action for the scalar

n(0^{++})	Soft-wall model		
	$\mu_G = 430$	$\mu_G = 600$	$\mu_G = 1000$
1	1216	1697	2828
2	1490	2078	3464
3	1720	2400	4000
4	1923	2683	4472

Table 2. 0^{++} glueball in the original soft-wall model. The unit is in MeV.

glueball $\mathscr{G}(x,z)$ in the string frame takes the form as that in the original soft-wall model [95, 96]

$$S_{\mathscr{G}} = \int d^5x\sqrt{g_s}\frac{1}{2}e^{-\Phi}\left[\partial_M\mathscr{G}\partial^M\mathscr{G} + M_{\mathscr{G},5}^2\mathscr{G}^2\right]. \tag{2.23}$$

The only difference is that the metric structure in the original soft-wall model is AdS_5, but in our dynamical soft-wall model the metric structure is selfconsistently solved from Section 2.1.

The Equation of motion for $\mathscr{G}$ has the form of

$$-e^{-(3A_s-\Phi)}\partial_z(e^{3A_s-\Phi}\partial_z\mathscr{G}_n) = m_{\mathscr{G},n}^2\mathscr{G}_n. \tag{2.24}$$

After the transformation $\mathscr{G}_n \to e^{-\frac{1}{2}(3A_s-\Phi)}\mathscr{G}_n$, we get the schrodinger like equation of motion for the scalar glueball

$$-\mathscr{G}_n'' + V_{\mathscr{G}}\mathscr{G}_n = m_{\mathscr{G},n}^2\mathscr{G}_n, \tag{2.25}$$

with the 5D effective schrodinger potential

$$V_{\mathscr{G}} = \frac{3A_s'' - \Phi''}{2} + \frac{(3A_s' - \Phi')^2}{4}. \tag{2.26}$$

2.2.1 Glueball spectra in original soft-wall model

In the original soft-wall model for glueball [95, 96], the dilaton background takes the quadratic form $\Phi = \mu_G^2 z^2$ but the metric structure is still AdS_5, one can easily derive the Regge spectra for scalar glueball:

$$m_{\mathscr{G},n}^{SW,2} = 4\mu_G^2(n+1),\ n = 1,2,\cdots \tag{2.27}$$

which implying that the Regge slope for the scalar glueball is $4\mu_G^2$, and the lightest glueball mass square is $8\mu_G^2$. In Table 2, we list some numerical results for the scalar glueball based on Eq. (2.27) with $\mu_G = 0.43, 0.6, 1\text{GeV}$, respectively.

From the lattice data for the scalar glueball as given in Table 1, one can read that the slope of the Regge spectra is around 4GeV^2, which means $\mu_G \simeq 1\text{GeV}$. From Eq. (2.27), the lightest scalar glueball mass square in the soft-wall model should be around

n(0^{++})	$\Phi = \mu_G^2 z^2$		
	$\mu_G = 900$	$\mu_G = 1000$	$\mu_G = 1100$
0	1434	1593	1752
1	2356	2618	2880
2	2980	3311	3642
3	3489	3877	4264

Table 3. 0^{++} glueball spectra in the soft-wall model with positive quadratic dilaton background $\Phi = \mu_G^2 z^2$ in unit of MeV.

$m^{2,AdS_5}_{\mathscr{G},n=1} \simeq 8\text{GeV}^2$, which is too large comparing with the lattice result $m^2_{\mathscr{G},n=1} \simeq 2 \sim 3\text{GeV}^2$. If one fixes the lightest scalar glueball mass square $m^{2,Lat}_{\mathscr{G},n=1} \simeq 2 \sim 3\text{GeV}^2$, which gives $\mu_G \simeq 0.5$ GeV, then the slope for the Regge spectra will be around 1 GeV^2, which is too small comparing with the lattice results 4 GeV^2.

In summary, by using the AdS$_5$ metric, the soft-wall model with the quadratic dilaton background field cannot accommodate both the lightest scalar glueball mass and the Regge slope.

2.2.2 Glueball spectra in quenched dynamical hQCD model

In the dynamical soft-wall (DSW) model, we firstly investigate the scalar glueball spectra with the positive quadratic dilaton background Eq.(2.17).

Under the boundary condition $\mathscr{G}_n(0) \to 0$ and $\mathscr{G}_n'(\infty) \to 0$, we get the scalar glueball spectra as shown in Table 3. It is observed that with 0.9 GeV $< \mu_G <$ 1.1 GeV, the scalar glueball spectra in the dynamical soft-wall model with positive quadratic dilaton background can fit lattice results quite well.

We would like to emphasize that the dynamical soft-wall model has the same parameters as the original soft-wall model, i.e. the AdS$_5$ radius L which is taken to be 1, and the quadratic coefficient of the dilaton background field μ_G. As we have shown in Sec.2.2.1, the original soft-wall model cannot accommodate both the ground state and the Regge slope. However, if one self-consistently solves the metric background under the dynamical dilaton field, it gives the correct ground state and at the same time gives the correct Regge slope. This is a surprise result! To explicitly see the difference, we show the scalar glueball spectra in the soft-wall model (blue dash-dotted line) and the dynamical soft-wall model (red solid line) in Fig. 1 for the case of $\mu_G = 1$GeV.

It is observed from Fig. 1 that the glueball spectra in the dynamical soft-wall model is parallel to that in the soft-wall model, and the separation is about $5.8\mu_G^2$. This indicates the ground sate of the scalar glueball has mass square around $m^2_{\mathscr{G},n=1} = 2.5\mu_G^2$, and has mass around $m_{\mathscr{G},n=1} = \sqrt{2.5}\mu_G$. From numerical results, we extract the Regge spectra in the dynamical soft-wall (DSW) model:

$$m^{2,DSW}_{\mathscr{G},n} = 4\mu_G^2(n-1) + 2.5\mu_G^2, \ n = 1, 2, \cdots \tag{2.28}$$

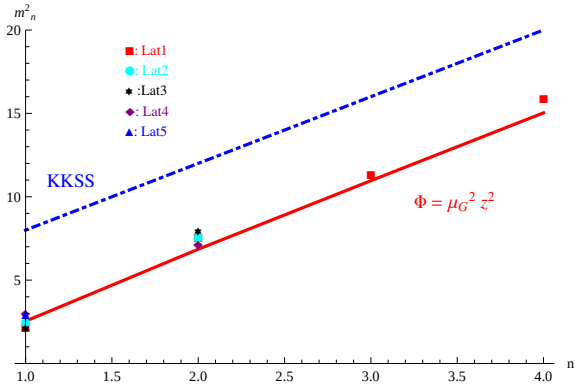

Figure 1. The 0^{++} glueball spectra for $\Phi = \mu_G^2 z^2$ with $\mu_G = 1\text{GeV}$ in the soft-wall model (blue dash-dotted line) and the dynamical soft-wall model (red solid line) and compare with lattice data.

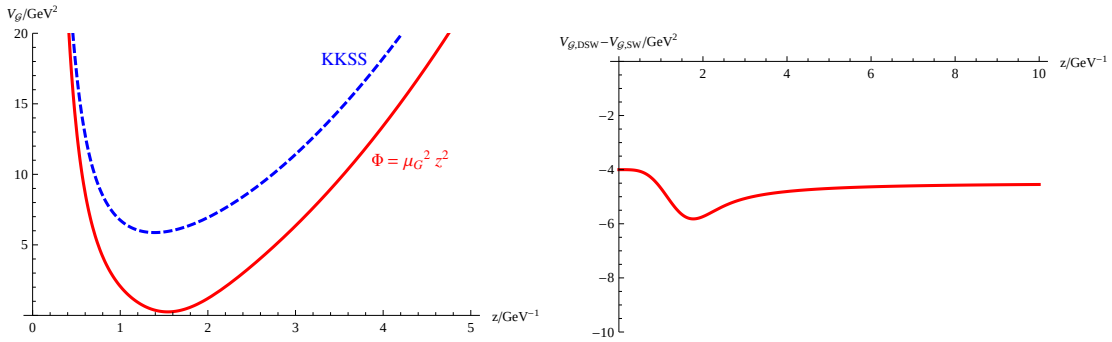

Figure 2. The potentials and their difference.

In order to understand the difference between the soft-wall model and the dynamical soft-wall model, we plot the effective schrodinger potentials $V_{\mathcal{G}}$ of the two models and their difference in Fig. 2. It is observed that the schrodinger potential $V_{\mathcal{G}}$ (red solid line) in the dynamical soft-wall model has a lower minimum than that in the soft-wall model (blue dashed line), the difference is about $5.8\mu_G^2$, which is the same as the difference of the mass square in these two models, i.e. $V_{\mathcal{G},DSW} - V_{\mathcal{G},SW} = m^2_{\mathcal{G},SW} - m^2_{\mathcal{G},DSW} = 5.8\mu_G^2$.

If the dynamical soft-wall model takes the negative quadratic dilaton background $\Phi = -\mu_G^2 z^2$, the metric structure has the form of Eq.(2.18), and the scalar glueball spectra is shown in Fig. 3 with $\mu_G = 0.43, 0.6, 1\text{GeV}$, respectively.

It is observed that the negative quadratic dilaton background can also generate the Regge spectra. However, like the soft-wall model, the dynamical soft-wall model with negative dilaton cannot accommodate both the ground state and the Regge slope.

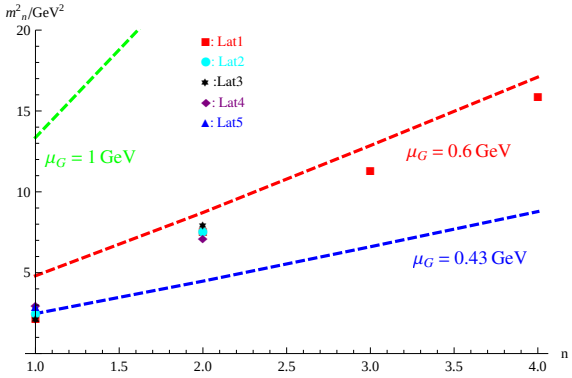

Figure 3. 0^{++} glueball in the dynamical soft-wall with negative quadratic background $\Phi = -\mu_G^2 z^2$ with $\mu_G = 0.43, 0.6, 1\text{GeV}$. The unit is in GeV and the dots are lattice data.

2.3 Linear quark potential in quenched dynamical soft-wall model

We follow the standard procedure [42, 99] to derive the static heavy quark potential $V_{Q\bar{Q}}(r)$ in the dynamical soft-wall holographic model under the general metric background Eq. (2.4). In SU(N) gauge theory, the interaction potential for infinity massive heavy quark antiquark is calculated from the Wilson loop

$$W[C] = \frac{1}{N}\text{Tr}P\exp[i\oint_C A_\mu dx^\mu], \tag{2.29}$$

where A_μ is the gauge field, the trace is over the fundamental representation, P stands for path ordering. C denotes a closed loop in space-time, which is a rectangle with one direction along the time direction of length T and the other space direction of length $R_{Q\bar{Q}}$.

The Wilson loop describes the creation of a $Q\bar{Q}$ pair with distance R at time $t_0 = 0$ and the annihilation of this pair at time $t = T$. For $T \to \infty$, the expectation value of the Wilson loop behaves as $\langle W(C)\rangle \propto e^{-TV_{Q\bar{Q}}}$. According to the *holographic* dictionary, the expectation value of the Wilson loop in four dimensions should be equal to the string partition function on the modified AdS_5 space, with the string world sheet ending on the contour C at the boundary of AdS_5

$$\langle W^{4d}[C]\rangle = Z^{5d}_{string}[C] \simeq e^{-S_{NG}[C]} \ , \tag{2.30}$$

where S_{NG} is the classical world sheet Nambu-Goto action

$$S_{NG} = \frac{1}{2\pi\alpha_p}\int d^2\eta\sqrt{\text{Det}\chi_{ab}}, \tag{2.31}$$

with α_p the 5D string tension which has dimension of GeV^{-2}, and χ_{ab} is the induced worldsheet metric with a, b the two indices of the world sheet coordinates (η^0, η^1). Without loss of generality, we can choose the $\eta^0 = t, \eta^1 = x$, and the position of one quark is $x = -\frac{R_{Q\bar{Q}}}{2}$ and the other is $x = \frac{R_{Q\bar{Q}}}{2}$. Under the background (2.4), the Nambu-Goto

action Eq.(2.31) becomes

$$S_{NG} = \frac{TL^2}{2\pi\alpha_p}\int dx e^{2A_s}\sqrt{1+z'^2}, \tag{2.32}$$

with the prime $'$ denotes the derivative with respective to x.

Since there's no dependence on x, we can easily obtain the equation of motion:

$$\frac{e^{2\mathcal{A}_s(z)}}{\sqrt{1+(z')^2}} = \text{Constant} = e^{2\mathcal{A}_s(z_0)}, \tag{2.33}$$

for the minimum world-sheet surface configuration.

Here the $R_{Q\bar{Q}}$ is dependent on z_0 which is the maximal value of z and $z'(x=0)=0$. For the configuration mentioned above and the given equation of motion, we impose the following boundary condtions $z(x=0)=z_0, z(x=\pm\frac{R_{qq}}{2})=0$. Following the standard procedure, one can derive the interquark distance $R_{Q\bar{Q}}$ as a function of z_0

$$R_{Q\bar{Q}}(z_0) = 2\int_0^{z_0} dz \frac{1}{\sqrt{1-\frac{b_s^4(z_0)}{b_s^4(z)}}}\frac{b_s^2(z_0)}{b_s^2(z)}. \tag{2.34}$$

The heavy quark potential can be worked out from the Nambu-Goto string action:

$$V_{Q\bar{Q}}(z_0) = \frac{g_p}{\pi}\int_0^{z_0} dz \frac{b_s^2(z)}{\sqrt{1-\frac{b_s^4(z_0)}{b_s^4(z)}}}, \tag{2.35}$$

with $g_p = \frac{L^2}{\alpha_p}$. It is noticed that the integral in Eq.(2.35) in principle include a pole in the UV region ($z\to 0$), which induces $V_{Q\bar{Q}}(z)\to\infty$. The infinite energy should be extracted through certain regularization procedure. The divergence of $V_{Q\bar{Q}}(z)$ is related to the vacuum energy for two static quarks. Generally speaking, the vacuum energy of two static quarks will be different in various background. In our latter calculations, we will use the regularized $V_{Q\bar{Q}}^{ren.}$, which means the vacuum energy has been subtracted. A minimal subtracted result related to the background solution Eq.(2.15) is as following,

$$V_{Q\bar{Q}}(z_0) = \frac{g_p}{\pi z_0}\left(\int_0^1 d\nu\left(\frac{b_s^2(z_0\nu)z_0^2}{\sqrt{1-\frac{b_s^4(z_0)}{b_s^4(z_0\nu)}}}-\frac{1}{\nu^2}\right)-1\right), \tag{2.36}$$

$$R_{Q\bar{Q}}(z_0) = 2z_0\int_0^1 d\nu \frac{1}{\sqrt{1-\frac{b_s^4(z_0)}{b_s^4(z_0\nu)}}}\frac{b_s^2(z_0)}{b_s^2(z_0\nu)}. \tag{2.37}$$

The integrate kernel in Eq.(2.36) has a pole at $\nu=1$, and by expanding the integral kernel at $\nu=1$ one has

$$1-\frac{b_s^4(z_0)}{b_s^4(z_0\nu)} = \frac{4z_0 b_s'(z_0)}{b_s(z_0)}(\nu-1)+o((\nu-1)^2)\,. \tag{2.38}$$

From Eqs.(2.36,2.37,2.38), we can find the necessary condition for the linear quark potential is that: There exists a point z_c, at which

$$b_s'(z_c)\to 0, b_s(z_c)\to const, \tag{2.39}$$

then the integral is dominated by $\nu = 1$ region, one can obtain the string tension

$$\sigma_s \propto \frac{V_{Q\bar{Q}}(z_0)}{R_{\bar{q}q}(z_0)} \overset{z_0 \to z_c}{\longrightarrow} \frac{g_p}{2\pi} b_s^2(z_c). \tag{2.40}$$

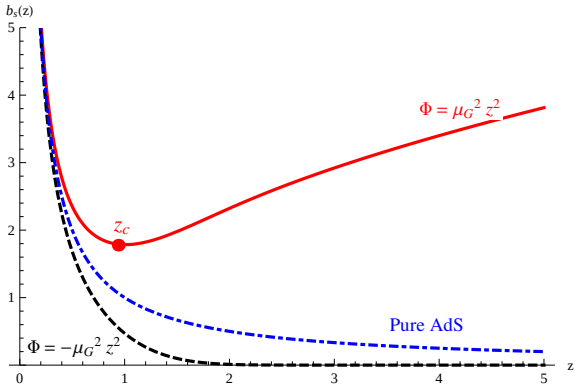

Figure 4. The metric structure $b_s(z) = e^{A_s(z)}$ as functions of z corresponding to the solution Eq.(2.17) for $\Phi = \mu_G^2 z^2$ (red solid line) and Eq.(2.18) for $\Phi = -\mu_G^2 z^2$ (black dashed line), respectively. The blue dash-dotted line stands for the pure AdS_5 case. $\mu_G = 1$GeV has been taken for numerical calculation.

Fig.4 shows the metric structure $b_s(z)$ as functions of z for the AdS_5 metric (blue dash-dotted line), and for the solutions Eq.(2.17) (red solid line) and Eq.(2.18) (black dashed line) of the quenched dynamical soft-wall model with positive and negative quadratic dilaton background fields $\Phi = \pm\mu_G^2 z^2$ respectively. We can see that only for the case of positive dilaton background $\Phi = \mu_G^2 z^2$, the metric solution Eq.(2.17) has a minimum point z_c. Therefore, the quark-antiquark potential should have a linear part for positive quadratic dilaton background $\Phi = \mu_G^2 z^2$, which can be seen explicitly from Fig.5. While for the pure AdS_5 case as well as for the dynamical soft-wall model with negative dilaton background field $\Phi = -\mu_G^2 z^2$, there doesn't exist a z_c where $b_s'(z_c) \to 0$, and correspondingly the heavy quark potential does not show a linear behavior at large z.

2.4 Short summary

In this section, we have modeled the pure gluon system by using the quenched dynamical soft-wall model in the graviton-dilaton framework. The quadratic dilaton background field Φ has dimension of 2, and Φ^2 is dual to the the dimension-4 gluon condensate. Comparing with the original soft-wall model with AdS_5 metric, here the metric background at IR is self-consistently deformed by the gluon condensate.

It is found that the positive quadratic dilaton background can give the correct glueball spectra including the Regge slope and ground state, as well as the linear quark potential, and the negative quadratic dilaton background field can be safely excluded. In the following study, we will only focus on the case of positive quadratic dilaton background.

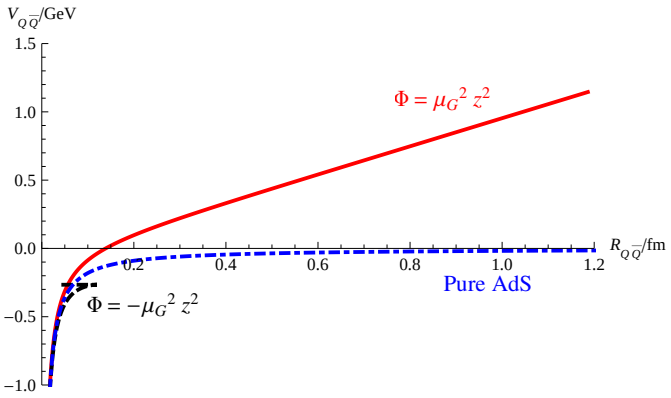

Figure 5. The quenched quark potential result $V_{Q\bar{Q}}$ as functions of $R_{Q\bar{Q}}$ in the quenched dynamical soft-wall mode with positive $\Phi = \mu_G^2 z^2$ (red solid line) and negative $\Phi = -\mu_G^2 z^2$ (black dashed line) quadratic dilaton background fields, respectively. The blue dash-dotted line stands for the pure AdS_5 case. $\mu_G = 1$GeV and $g_p = 0.4$ have been used for numerical calculations.

3 Two flavor system: KKSS model and improved KKSS model

We now turn to the the light flavor system with chiral symmetry $SU(2)_L \times SU(2)_R$. As we have mentioned in the Introduction, the current achievements of AdS/QCD models for hadron spectra are the hard-wall AdS/QCD model [21] and the soft-wall AdS/QCD or KKSS model [22] and its extended version [34–36]. In the hard-wall model [22], the chiral symmetry breaking can be realized by chiral condensation in the vacuum, however, the resulting mass spectra for the excited mesons behave as $m_n^2 \sim n^2$, which is different from the linear Regge behavior $m_n^2 \sim n$. In order to generate the linear Regge behavior, the authors of Ref.[22] introduced a quadratic dilaton background, one can obtain a desired mass spectra for the excited vector mesons, while the chiral symmetry breaking phenomenon cannot consistently be realized. In the following, we firstly give a brief introduction on the KKSS model and review the meson spectra in this model.

3.1 The KKSS model

The KKSS model [22] have two background fields: the positive quadratic dilaton background $\Phi = \mu^2 z^2$ and the metric background g_{MN}. Note, in the following, we will use μ instead of μ_G to distinguish from the pure gluon system. The background geometry is not dynamically generated but assumed to be AdS_5 space with the metric structure

$$ds^2 = g_{MN} dx^M dx^N = \frac{L^2}{z^2}\left(\eta_{\mu\nu} dx^\mu dx^\nu + dz^2\right), \tag{3.1}$$

which gives $A_s(z) = -\log(z/L)$.

The mesons are described by 5D fields propagating on the background with the action given by

$$S_{\rm KKSS} = -\int d^5x e^{-\Phi(z)} \sqrt{g_s} Tr\Big(|DX|^2 + m_X^2 X^2 + \frac{1}{4g_5^2}(F_L^2 + F_R^2)\Big), \tag{3.2}$$

with $g_5 = 12\pi^2/N_c$. The scalar field X is dual to the dimension-3 $q\bar{q}$ operator, and m_X is the 5D scalar mass. According to AdS/CFT dictionary, the dimension-3 scalar has 5D mass $m_X^2 = -3$. The field $X(z)$ is actually a complex field to incorporate the scalar S and the pseudoscalar P fields,

$$X^{\alpha\beta}(z) = \left(\frac{\chi(z)}{2} + S\right) 1^{\alpha\beta} \mathrm{e}^{iP^a t^a}, \tag{3.3}$$

where α, β are in the isospin space, $a = 1, 2, 3$ are the $SU(2)$ generator index. The scalar field takes a nonzero vacuum expectation value (VEV) $\chi(z)$, which is expected to realize the chiral symmetry breaking.

The Gauge fields L_M and R_M model the SU(2)$_L\times$ SU(2)$_R$ global chiral symmetry of QCD for two flavors of quarks, which are defined as

$$\begin{aligned} F_L^{MN} &= \partial^M L^N - \partial^N L^M - i[L^M, L^N], \\ F_R^{MN} &= \partial^M R^N - \partial^N R^M - i[R^M, R^N], \end{aligned} \tag{3.4}$$

where $L^M = L^{Ma} t^a$ and $\mathrm{Tr}[t^a t^b] = \delta^{ab}/2$. The covariant derivative becomes

$$D^M X = \partial^M X - iL^M X + iXR^M. \tag{3.5}$$

To describe the vector and axial-vector fields, we simply transform the L and R gauge fields into the vector (V) and axial-vector (A) fields with $L^M = V^M + A^M$ and $R^M = V^M - A^M$, one can have $F_L^2 + F_R^2 = 2\left(F_V^2 + F_A^2\right)$, with

$$F_V^{MN} = \partial^M V^N - \partial^N V^M - \frac{i}{\sqrt{2}}[V^M, V^N], \tag{3.6}$$

$$F_A^{MN} = \partial^M A^N - \partial^N A^M - \frac{i}{\sqrt{2}}[A^M, A^N]. \tag{3.7}$$

In terms of the vector V and axial-vector A fields, the KKSS action Eq.(3.2) can be rewritten as

$$S_{KKSS} = -\int d^5x \sqrt{g_s}\, \mathrm{e}^{-\Phi(z)} \mathrm{Tr}\left[|DX|^2 + m_X^2 |X|^2 + \frac{1}{2g_5^2}(F_V^2 + F_A^2)\right], \tag{3.8}$$

where the covariant derivative now becomes

$$D^M X = \partial^M X - i[V^M, X] - i\{A^M, X\}. \tag{3.9}$$

3.2 Degeneration of chiral partners in KKSS model

The scalar field takes a nonzero vacuum expectation value (VEV) $\chi(z)$, which is expected to realize the chiral symmetry breaking as in the hard wall model. We will show in the following that the chiral symmetry breaking is not realized in the soft-wall model or KKSS model, and we will analyze the reason.

Scalar vacuum expectation value

The equation of motion for the scalar vacuum expectation value (VEV) $\chi(z)$ defined in Eq.(3.3) can be deduced and takes the following form,

$$\chi^{''} + (3A_s^{'} - \Phi^{'})\chi^{'} - m_X^2 e^{2A_s}\chi = 0. \tag{3.10}$$

In the hard wall model, $\Phi^{'} = 0$, the scalar VEV has the exact solution

$$\chi(z) = c_1 z + c_2 z^3 = m_q z + \sigma z^3, \tag{3.11}$$

where we have identified $m_q = c_1$ and $\sigma =< \bar{q}q >= c_2$. In the softwall model, $\Phi(z) = \mu^2 z^2$ and $\Phi^{'} = 2\mu^2 z$, and the general solution of Eq.(3.10) has the form of

$$\chi(z) = c_2 G_{1,2}^{2,0}\left(-z^2 \Big|\begin{matrix}1\\ \frac{1}{2},\frac{3}{2}\end{matrix}\right) + c_1 e^{\frac{z^2}{2}} z^3\left(I_0\left(\frac{z^2}{2}\right) + I_1\left(\frac{z^2}{2}\right)\right). \tag{3.12}$$

with $I_n(z)$ the modified Bessel function of the first kind,$G_{pq}^{mn}\left(z\left|\begin{matrix}a_1,\ldots,a_p\\ b_1,\ldots,b_q\end{matrix}\right.\right)$ the MeijerG function(For details, please refer to Mathematica 8.0).

To be more instructive, we can extract the large z behavior of χ from the equation of motion : assuming $\chi^{''} << \chi$,when $z >> 1$, we have $-2\mu^2 z\chi^{'} + 3\chi/z^2 = 0$, and assuming $\chi^{'} >> \chi$,when $z >> 1$, we have $\chi^{''} - 2\mu^2 z\chi^{'} = 0$. And then we could get the IR behaviors of the two independent solution: $\chi_1 \to e^{\mu^2 z^2}/(\mu z)$ and $\chi_2 \to e^{-3/(4\mu^2 z^2)} \to 1$. The first one would make the spectra of a_1 nonlinear, so in order to produce linear a_1 spectra, c_1, c_2 in Eq.(3.10) are not independent. Requiring $\chi \propto \chi_2(z)$, when $z >> 1$, the small z expansion of χ would be:

$$\chi(z) = c(\mu z + \mu^3 z^3\left(-\frac{1}{2} + \gamma_E + \frac{\psi\left(-\frac{1}{2}\right)}{2} + \log(\mu z)\right)) + O(z^4) \tag{3.13}$$

$$= c(\mu z + \mu^3 z^3(0.095 + \log(\mu z))) \tag{3.14}$$

with $\gamma_E = 0.577$ the Euler's constant and $\psi(z)$ the digmma function with $\psi(-\frac{1}{2}) = 0.036$. We would take $c = m_q/\mu$, so σ can be read as $\sigma = 0.095 m_q \mu^2$. The experimental data for vector, axialvector, scalar and pseudoscalar are shown in Table 4. To fit the Regge slope of vector meson ρ, we have to choose $\mu = 0.43$. Then even we take $m_q = 9$MeV, σ is only (54 MeV)^3, which is too small comparing with the experienced value (250 MeV)^3. This problem was pointed in the original paper and the authors also mentioned to add quartic terms $|X|^4$ to cure it.

Meson spectra

In the following, we show the meson spectra in the KKSS model. The equations of motion of the vector, axial-vector, scalar and pseudo-scalar mesons take the form of:

$$-\rho_n^{''} + V_\rho \rho_n = m_n^2 \rho_n, \tag{3.15}$$

$$-a_n^{''} + V_a a_n = m_n^2 a_n, \tag{3.16}$$

$$-s_n^{''} + V_s s_n = m_n^2 s_n, \tag{3.17}$$

$$-\pi_n'' + V_{\pi,\varphi}\pi_n = m_n^2(\pi_n - e^{A_s}\chi\varphi_n),$$

$$-\varphi_n'' + V_\varphi \varphi_n = g_5^2 e^{A_s}\chi(\pi_n - e^{A_s}\chi\varphi_n). \tag{3.18}$$

Exp.	n	ρ (MeV)	a_1 (MeV)	f_0 (MeV)	π (MeV)
	1	775 ± 1	1230 ± 40	550^{+250}_{-150}	140
	2	1282 ± 37	1647 ± 22	980 ± 10	1300 ± 100
	3	1465 ± 25	1930^{+30}_{-70}	1350 ± 150	1816 ± 14
	4	1720 ± 20	2096 ± 122	1505 ± 6	2070
	5	1909 ± 30	2270^{+55}_{-40}	1724 ± 7	2360
	6	2149 ± 17	—-	1992 ± 16	—-
	7	2265 ± 40	—-	2103 ± 8	—-
	8	—-	—-	2314 ± 25	—-

Table 4. The experimental data for meson mass from PDG [31]. The data selection scenario used here is the same as in Ref.[35], which shows the chiral symmetry breaking maintains in the highly excited states of chiral partners.

KKSS	n	ρ (MeV)	a_1 (MeV)	f_0 (MeV)	π (MeV)
	1	860	860	1053	1054
	2	1216	1217	1360	1360
	3	1489	1490	1609	1609
	4	1720	1720	1824	1824
	5	1923	1923	2017	2017
	6	2107	2107	2193	2192
	7	2275	2275	2355	2355

Table 5. The mass spectra for vector mesons ρ, axial vector mesons a_1, scalar mesons f_0 and pseudoscalar mesons π in the KKSS model with $m_q = 9$ MeV, $\mu = 430$ MeV, which gives $\sigma = (54 \text{ MeV})^3$).

with schrodinger like potentials

$$V_\rho = \frac{A_s^{'} - \Phi^{'}}{2} + \frac{(A_s^{'} - \Phi^{'})^2}{4}, \tag{3.19}$$

$$V_a = \frac{A_s^{'} - \Phi^{'}}{2} + \frac{(A_s^{'} - \Phi^{'})^2}{4} + g_5^2 e^{2A_s}\chi^2, \tag{3.20}$$

$$V_s = \frac{3A_s^{''} - \phi^{''}}{2} + \frac{(3A_s^{'} - \phi^{'})^2}{4} - m_\chi^2 e^{2A_s}, \tag{3.21}$$

$$V_{\pi,\varphi} = \frac{3A_s^{''} - \Phi^{''} + 2\chi^{''}/\chi - 2\chi^{'2}/\chi^2}{2} + \frac{(3A_s^{'} - \Phi^{'} + 2\chi^{'}/\chi)^2}{4}, \tag{3.22}$$

$$V_\varphi = \frac{A_s^{''} - \Phi^{''}}{2} + \frac{(A_s^{'} - \Phi^{'})^2}{4}. \tag{3.23}$$

Since $g_5^2 e^{2A_s}\chi^2 \to 0$ when $z \to \infty$, we can expect the spectra of the chiral partners, i.e. the vector and axial vector as well as the scalar and pseudoscalar mesons would be degenerate

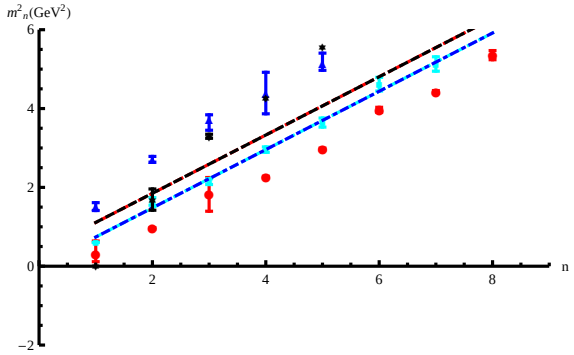

Figure 6. Meson spectra in the KKSS model with $m_q = 9$ MeV, $\mu = 430$ MeV comparing with experimental data in Table 4.

in the large n region.

The meson spectra in the KKSS model is shown in Table 5 and Fig.6. In order to realize the linear Regge behavior, we have used parameters $m_q = 9$ MeV, $\mu = 430$ MeV. However, this gives a small chiral condensate $\sigma = (54\text{MeV})^3$, which leads to the degeneration of chiral partners, i.e. the scalar spectra overlaps with the pseudoscalar spectra, and the vector spectra overlaps with the axial-vector spectra. On the other hand, in order to realize the chiral symmetry breaking in the KKSS model, i.e. the separation of the spectra of the chiral partners, as shown in [33], one cannot get the linear Regge behavior for the axial-vector meson.

3.3 Improved KKSS model with quartic interaction term

As we have shown above that the KKSS model cannot accommodate chiral symmetry breaking and linear confinement. Refs. [34, 35] introduced a quartic interaction term κX^4 in the bulk scalar potential to improve the situation. Nevertheless, such a term was shown in Ref. [35] by Gherghetta-Kapusta-Kelley to result in a negative mass for the lowest lying scalar meson state.

The meson spectra in the Gherghetta-Kapusta-Kelley (GKK) model is shown in Fig.7, where the parameters are chosen: $m_q = 9.75\text{MeV}, \sigma = (204.5\text{ MeV})^3, \mu = 430$ MeV (equivalent to $\lambda = 0.183 GeV^2$ in their notation). The lowest scalar meson has mass square $m^2_{f_0,n=1} = -0.559\text{GeV}^2$, which shows the instability in the scalar sector.

3.4 Improved KKSS model with deformed warp factor

In Ref.[36], Sui-Wu-Xie-Yang (SWXY) introduced a deformed warp factor in the KKSS and GKK model and the metric structure takes the form of

$$b_s(z) = \frac{1 + \mu_g^2 z^2}{z^2}, \tag{3.24}$$

which can cure the instability of the scalar potential and produce meson spectra in good agreement with experimental data. Even though the authors in Ref.[36] didn't calculate

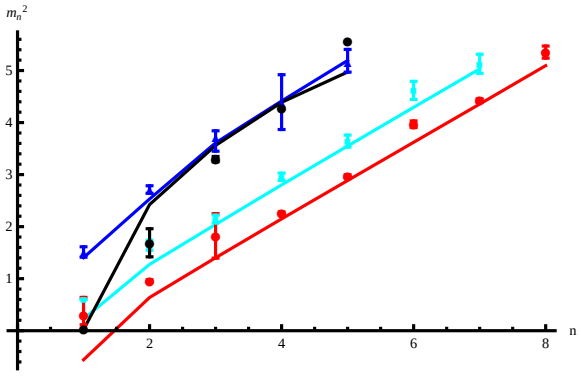

Figure 7. Meson spectra in the GKK model with $m_q = 9.75$ MeV, $\sigma = (204.5 \text{ MeV})^3$, $\mu = 430$ MeV.

the heavy quark potential, but from our criteria for the linear quark potential Eq. (2.39), the geometric factor Eq.(3.24) in the SWXY model can produce a linear potential.

In this model, the authors grouped their settings into "case-a" and "case-b".

1) In "case-a", the large z behavior of the scalar (see Eq.(9) in their paper) is $\chi(z \to \infty) = \gamma(\mu z)$, since their metric warp factor is like $A_s(z \to \infty) = constant$, the difference between the effective potential in vector sector and axial-vector sector takes the limit of $g_5^2 \chi^2 e^{2A_s} \propto z^2$, we can see the Regge slope for the vector spectra is different from that for the axial-vector mesons.

2) In "case-b", $\chi(z \to \infty) = \gamma(\sqrt{\mu z})$, the difference between the effective potential in vector sector and axial-vector sector takes the limit of $g_5^2 \chi^2 e^{2A_s} \propto z$, and the vector and axial-vector spectra would approach each other at high excitations.

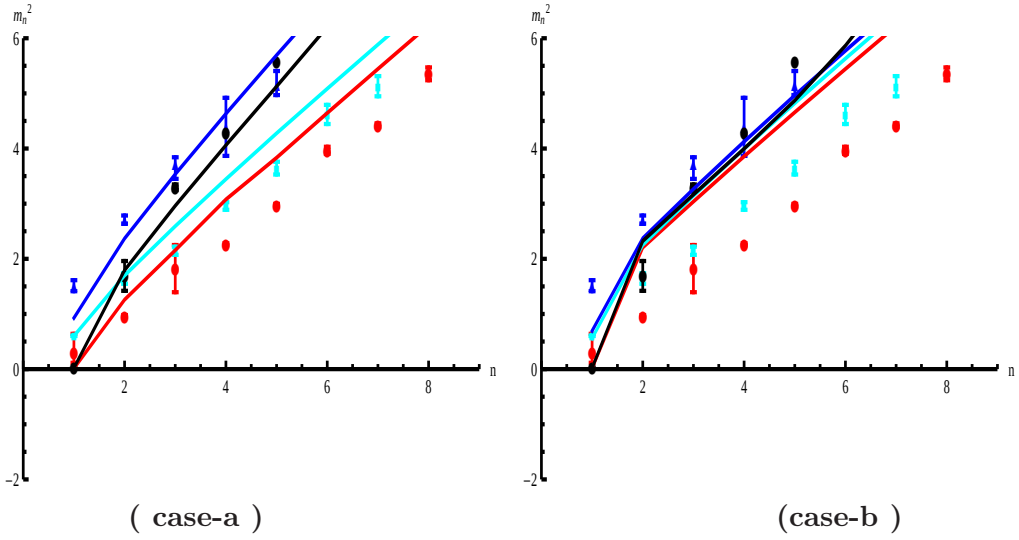

Figure 8. Meson spectra in the SWXY model comparing with experimental data in Table 4. The parameters $\mu = 445$MeV (their μ_d), and $m_q = 4.98$MeV, $\sigma = (255\text{MeV})^3$ are used for case-a, and $m_q = 4.25$MeV, $\sigma = (268\text{MeV})^3$ are used for case-b.

The meson spectra for the SWXY model are shown in Fig.8(we only take the Model III in their original paper as an example), where for case-a(their IIIa) they have used parameters as $\mu = 445\text{MeV}, m_q = 4.98\text{MeV}, \sigma = (255\text{MeV})^3$, and for case-b(their IIIb), they have use parameters as $\mu = 445\text{MeV}, m_q = 4.25\text{MeV}, \sigma = (268\text{MeV})^3$. It is found that for case-a, the Regge slopes for the scalar and vector meson spectra are the same, and the Regge slopes for the pseudo-scalar and axial-vector meson spectra are the same, while the slopes of the two groups are different. For case-b, all spectra are degenerate.

It is worthy of mentioning that the meson spectra are compared with experimental data taken in Table 4, which are the same as in Ref. [35], and different from the experimental data taken in Ref. [36]. As for which data should be taken properly, and whether there should be chiral symmetry restoration at high excitation states [33, 100, 101], we leave them as open questions.

4 Two flavor system: the dynamical soft-wall model

A successful holographic QCD model should describe chiral symmetry breaking, and at the same time should describe both the Regge trajectories of hadron spectra and linear quark potential, two aspects in the manifestation of color confinement. Thus how to naturally incorporate all these important features into a single AdS/QCD model and obtain the consistent mass spectra remains a challenging and interesting task. In this section, we provide a fully dynamical soft-wall holographic QCD model formulated in the graviton-dilaton-scalar system, which can incorporate chiral symmetry breaking, Regge spectra as well as linear quark potential.

4.1 Dynamical soft-wall model: the graviton-dilaton-scalar system

As we have shown in Sec. II that the pure gluodynamics can be described very well by the quenched dynamical soft-wall model formulated in the graviton-dilaton system. The quadratic dilaton background related to the gluon condensate in the vacuum can produce the linear confinement, including linear Regge spectra and the linear heavy quark potential. We now add light flavors in terms of meson fields on the gluodynamical background. The total 5D action for the graviton-dilaton-scalar system takes the following form:

$$S = S_G + \frac{N_f}{N_c} S_{KKSS}, \tag{4.1}$$

with

$$S_G = \frac{1}{16\pi G_5}\int d^5x\sqrt{g_s}e^{-2\Phi}\big(R + 4\partial_M\Phi\partial^M\Phi - V_G(\Phi)\big), \tag{4.2}$$

$$S_{KKSS} = -\int d^5x\sqrt{g_s}e^{-\Phi}Tr(|DX|^2 + V_X(X^+X,\Phi) + \frac{1}{4g_5^2}(F_L^2 + F_R^2)). \tag{4.3}$$

It is noticed that S_G is the 5D action for gluons in terms of dilaton field Φ and takes the same form as Eq.(2.3), here we have assumed the action is in the string frame. S_{KKSS} is the 5D action for mesons propagating on the dilaton background and takes the same form as the general KKSS action Eq.(3.2). $V_G(\Phi)$ and $V_X(X^+X,\Phi)$ are potentials for dilaton field and scalar field, respectively. It is noticed that the scalar field might mix with the gluon fields, therefore we have chosen a general form for the scalar potential $V_X(X^+X,\Phi)$.

4.2 Background fields in the vacuum with chiral and gluon condensate

In the vacuum, it is assumed that there are both gluon condensate and chiral condensate. The square of the dilaton background field Φ^2 is supposed to be dual to the gauge invariant dimension-4 gluon condensate $< G^2 >$. In order to distinguish the dilaton background from the pure gluon system, we take the positive quadratic dilaton background with a different coefficient

$$\Phi = \mu^2 z^2. \tag{4.4}$$

The scalar field $X(z)$ is a complex field as shown in Eq.(3.3) and it is expected that the scalar field takes a nonzero vacuum expectation value (VEV) $\chi(z)$.

It's easy to get the 5D action for the vacuum background:

$$S_{vac} = S_{G,vac} + \frac{N_f}{N_c} S_{KKSS,vac}, \tag{4.5}$$

with

$$S_{G,vac} = \frac{1}{16\pi G_5}\int d^5x\sqrt{g_s}e^{-2\Phi}\big(R + 4\partial_M\Phi\partial^M\Phi - V_G(\Phi)\big) \tag{4.6}$$

$$S_{KKSS,vac} = -\int d^5x\sqrt{g_s}e^{-\Phi}(\frac{1}{2}\partial_M\chi\partial^M\chi + V_C(\chi,\Phi)) \tag{4.7}$$

where we have defined $V_C = Tr(V_X)$ For further convenience, we define

$$V_{C,\chi} = \frac{\partial V_C}{\partial\chi}, \quad V_{C,\chi\chi} = \frac{\partial^2 V_C}{\partial^2\chi}. \tag{4.8}$$

By Redefinition: $L^{\frac{3}{2}}\chi \to \chi, L^3 V_C \to V_C, \frac{16\pi G_5 N_f}{L^3 N_c} \to \lambda$ we can set all the fields and constants to be dimensionless, and the vacuum action takes the form of

$$S_{vac} = \frac{1}{16\pi G_5}\int d^5x \ \ \sqrt{g_s}\big\{e^{-2\Phi}[R + 4\partial_M\Phi\partial^M\Phi - V_G(\Phi)] \\ -\lambda e^{-\Phi}(\frac{1}{2}\partial_M\chi\partial^M\chi + V_C(\chi,\Phi))\big\} \tag{4.9}$$

After the frame transformation $g^s_{MN} = g^E_{MN}e^{\frac{2}{3}\Phi}$, the action S_{vac} in the Einstein frame takes the following form

$$S_{vac} = \frac{1}{16\pi G_5}\int d^5x \ \ \sqrt{g_E}\big\{[R_E - \frac{4}{3}\partial_M\Phi\partial^M\Phi - V^E_G(\Phi)] \\ -\lambda e^{\Phi}(\frac{1}{2}\partial_M\chi\partial^M\chi + e^{\frac{4}{3}\Phi}V_C(\chi,\Phi))\big\}. \tag{4.10}$$

The Einstein equation and field equations in the Einstein frame have the expression of

$$E_{MN} + \frac{1}{2}g^E_{MN}\left(\frac{4}{3}\partial_l\Phi\partial^l\Phi + V^E_G(\Phi) + \lambda(\frac{1}{2}e^{\Phi}\partial_l\chi\partial^l\chi + e^{\frac{7}{3}\Phi}V_C(\chi,\Phi))\right) \tag{4.11}$$

$$-\frac{4}{3}\partial_M\Phi\partial_N\Phi - \frac{\lambda}{2}e^{\Phi}\partial_M\chi\partial_N\chi = 0, \tag{4.12}$$

$$\frac{8}{3\sqrt{g_E}}\partial_M(\sqrt{g_E}\partial^M\Phi) - \lambda\frac{1}{2}e^{\Phi}\partial_M\chi\partial^M\chi - \partial_\Phi\left(V_G(\Phi) + \lambda e^{\frac{7}{3}\Phi}V_C(\chi,\Phi)\right) = 0, \tag{4.13}$$

$$\lambda\frac{1}{\sqrt{g_E}}\partial_M(\sqrt{g_E}e^{\Phi}\partial^M\chi) - \partial_\chi\left(V_G(\Phi) + \lambda e^{\frac{7}{3}\Phi}V_C(\chi,\Phi)\right) = 0. \tag{4.14}$$

We can derive the three coupled field equations in the string frame as

$$-A_s'' + A_s'^2 + \frac{2}{3}\Phi'' - \frac{4}{3}A_s'\Phi' - \frac{\lambda}{6}e^{\Phi}\chi'^2 = 0, \tag{4.15}$$

$$\Phi'' + (3A_s' - 2\Phi')\Phi' - \frac{3\lambda}{16}e^{\Phi}\chi'^2 - \frac{3}{8}e^{2A_s - \frac{4}{3}\Phi}\partial_\Phi\left(V_G(\Phi) + \lambda e^{\frac{7}{3}\Phi}V_C(\chi,\Phi)\right) = 0, \tag{4.16}$$

$$\chi'' + (3A_s' - \Phi')\chi' - e^{2A_s}V_{C,\chi}(\chi,\Phi) = 0. \tag{4.17}$$

If we know the form of the dilaton field Φ and the scalar field χ, then the metric A_s, the dilaton potential $V_G(\Phi)$ and the scalar potential $V_C(\chi,\Phi)$ should be self-consistently solved from the above three coupled equations.

4.3 Chiral symmetry breaking and linear confinement

In the case of positive quadratic dilaton background $\Phi(z) = \mu^2 z^2$, we will constrain the form of scalar VEV from the linear confinement.

The UV asymptotic form of $\chi(z)$

As proposed in the KKSS model, at the ultraviolet(UV) region, the scalar field takes the following asymptotic form,

$$\chi(z) \xrightarrow{z\to 0} m_q\zeta z + \frac{\sigma}{\zeta}z^3, \tag{4.18}$$

where m_q is the current quark mass, and σ is the quark antiquark condensate, and ζ is a normalization constant and is fixed as $\zeta^2 = \frac{N_c^2}{4\pi^2 N_f}$ with $N_c = 3, N_f = 2$.

The IR asymptotic form of $\chi(z)$ constrained from linear quark potential

The linear behavior of quark-antiquark static potential in the heavy quark mass limit $m_Q \to \infty$ can describe the permanent confinement property of QCD. In Sec. 2.3, we have derived the heavy quark potential under the general metric background A_s, and we have observed that for the metric structure $b_s = e^{A_s}$, if there exists a point z_c where $b_s^{'}(z_c) \to 0$, then one can extract the string tension σ_s of the linear potential as

$$\sigma_s = \frac{V_{\bar{q}q}(z_0)}{R_{\bar{q}q}(z_0)} \overset{z_0 \to z_c}{\longrightarrow} \frac{g_p}{2\pi} b_s^2(z_c). \tag{4.19}$$

Therefore, the necessary condition for the linear part of the $Q - \bar{Q}$ potential is that there exists one point z_c or one region, where $b_s^{'}(z) \to 0, z \to z_c$ while $b_s(z)$ keeps finite. For simplicity, we can take the following constraint on the metric structure at IR:

$$A_s^{'}(z) \overset{z \to \infty}{\longrightarrow} 0, A_s(z) \overset{z \to \infty}{\longrightarrow} \text{Const.} \tag{4.20}$$

Under the condition of Eq.(4.20), the equation of motion Eq.(4.15) in the IR takes the following simple form:

$$\frac{2}{3}\Phi'' - \frac{\lambda}{6} e^{\Phi} \chi'^2 = 0, \tag{4.21}$$

which provides a relation between the chiral condensate and low energy gluodynamics at IR. The asymptotic form of $\chi(z)$ at IR can be solved as:

$$\chi(z) \overset{z \to \infty}{\longrightarrow} \sqrt{8/\lambda}\mu e^{-\Phi/2}. \tag{4.22}$$

The full form of $\chi(z)$

To match the asymptotic forms both at UV and IR in Eqs.(4.18) and (4.22), χ can be parameterized as

$$\chi^{'}(z) = \sqrt{8/\lambda}\mu e^{-\Phi/2}(1 + c_1 e^{-\Phi} + c_2 e^{-2\Phi}), \tag{4.23}$$

with $c_1 = -2 + \frac{5\sqrt{2\lambda} m_q \zeta}{8\mu} + \frac{3\sqrt{2\lambda}\sigma}{4\zeta\mu^3}$, and $c_2 = 1 - \frac{3\sqrt{2\lambda} m_q \zeta}{8\mu} - \frac{3\sqrt{2\lambda}\sigma}{4\zeta\mu^3}$. Solving Eq.(4.23), we can obtain the full expression for the scalar VEV, which takes the following form:

$$\begin{aligned}
\chi(z) = \; & \frac{1}{30\zeta\mu^3}\sqrt{\frac{\pi}{2\lambda}}\Big(5\sqrt{3}\text{Erf}\left(\sqrt{\frac{3}{2}}\mu z\right)\left(-8\sqrt{2}\zeta\mu^3 + 6\sqrt{\lambda}\sigma + 5\zeta^2\sqrt{\lambda}\mu^2 m_q\right) \\
& + 3\Big(\sqrt{5}\text{Erf}\left(\sqrt{\frac{5}{2}}\mu z\right)\left(4\sqrt{2}\zeta\mu^3 - 6\sqrt{\lambda}\sigma - 3\zeta^2\sqrt{\lambda}\mu^2 m_q\right) \\
& + 20\sqrt{2}\zeta\mu^3 \text{Erf}\left(\frac{\mu z}{\sqrt{2}}\right)\Big)\Big),
\end{aligned} \tag{4.24}$$

where $g_5^2 = 4\pi^2 \frac{N_f}{N_c}$ and $\zeta^2 = \frac{N_c^2}{4\pi^2 N_f}$.

With the input of $\Phi(z) = \mu^2 z^2$ and $\chi(z)$ given in Eq.(4.24), one can solve the metric A_s or b_s from the equation of motion Eq. (4.15). By taking $G_5 = \frac{3L^3}{4}, m_q = 5$ MeV$, \sigma =$ (240 MeV)^3, we show the numerical results for the scalar VEV $\chi(z)$ and the solved metric structure $b_s(z)$ in Fig.9.

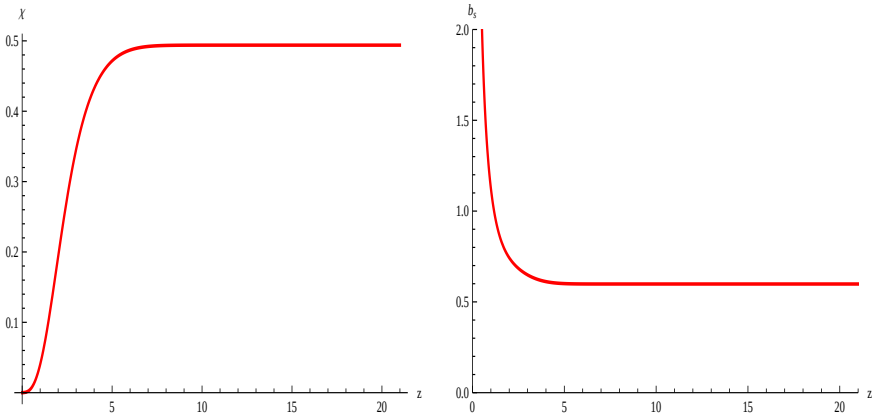

Figure 9. Scalar VEV $\chi(z)$ and solved metric structure b_s as functions of z with $G_5 = \frac{3L^3}{4}, m_q =$ 5 MeV$, \sigma =$ (218 MeV)^3.

The heavy quark potential under the solved metric structure is also shown in Fig. 10 by the solid line and comparing with the Cornell potential $V^{Cornell}(R) = -\frac{\kappa}{R} + \sigma_s R + V_0$ with $\kappa \approx 0.48$, $\sigma_s \approx 0.183\text{GeV}^2$ and $V_0 = -0.25$GeV. It is observed that the heavy quark potential produced in our model including the back-reaction from light flavor dynamics agree well with the Cornell potential.

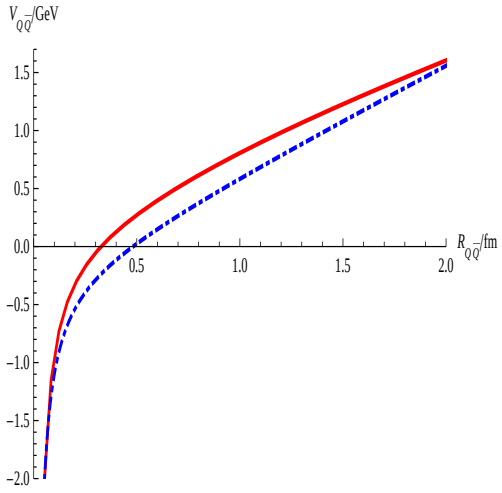

Figure 10. Heavy quark potential $V_{Q\bar{Q}}$ as a function of $R_{Q\bar{Q}}$ from our model (solid line) with $g_p = 2.3$ and $\mu = 430\text{MeV}, \sigma = (218\text{MeV})^3$ compared with the Cornell potential (dot-dashed line).

4.4 Meson spectra in the graviton-dilaton-scalar system

With the dilaton background field $\Phi(z) = \mu^2 z^2$ and the scalar background field $\chi(z)$ given in Eq.(4.24), we have solved the metric A_s or b_s from the equation of motion Eq. (4.15). Now we are ready to derive the meson spectra in the dynamical soft-wall model.

4.4.1 Scalar spectra

The action of the scalar perturbation is

$$S_s = -2\frac{N_f}{N_c L^3}\int d^5x e^{-\Phi}\sqrt{g_s}(\partial_z S\partial^z S + \partial_\mu S\partial^\mu S + V_{C,\chi\chi}(\chi,\Phi)S^2), \tag{4.25}$$

and the equation of motion for the scalar perturbation after doing the KK modes expansion is

$$-e^{-(3A_s-\Phi)}\partial_z(e^{3A_s-\Phi}\partial_z s_n) + e^{2A_s}V_{C,\chi\chi}(\chi,\Phi)s_n = m_n^2 s_n. \tag{4.26}$$

By doing the transformation $s_n \to s_n e^{-(3A_s-\Phi)/2}$, one can get the schrodinger like equation

$$-s_n^{''} + V_s(z)s_n = m_n^2 s_n \tag{4.27}$$

with the schrodinger potential

$$V_s(z) = \frac{3A_s^{''} - \Phi^{''}}{2} + \frac{(3A_s^{'} - \Phi^{'})^2}{4} + e^{2A_s}V_{C,\chi\chi}(\chi,\Phi). \tag{4.28}$$

Assuming the scalar potential can be separated into

$$V_C(\chi,\Phi) = e^{f(\Phi)}V_c(\chi), \tag{4.29}$$

	G_5/L^3	m_q (MeV)	$\sigma^{1/3}$ (MeV)
Mod I	0.75	5	218
Mod II	0.75	5	240

Table 6. Two sets of parameters.

we have

$$e^{2A_s}V_{C,\chi\chi} = e^{2A_s+f(\Phi)}V_{c,\chi\chi} = e^{2A_s+f(\Phi)}\frac{\partial_z(V_{c,\chi})}{\chi^{'}} \tag{4.30}$$

By using Eq.(4.17), we can have

$$\begin{aligned} e^{2A_s}V_{C,\chi\chi} &= e^{2A_s+f(\Phi)}\frac{\partial_z(e^{-(2A_s+f(\Phi))}(\chi^{''}+(3A_s^{'}-\Phi^{'})\chi^{'}))}{\chi^{'}} \\ &= \frac{\chi^{'''}}{\chi^{'}} + (A_s^{'}-\Phi^{'}-f_{,\Phi}\Phi^{'})\frac{\chi^{''}}{\chi^{'}} + 3A_s^{''} - \Phi^{''} \\ &-(2A_s^{'}+f_{,\Phi}\Phi^{'})(3A_s^{'}-\Phi^{'}). \end{aligned} \tag{4.31}$$

In our solution, $\chi^{'}(z) \propto e^{-\frac{1}{2}\Phi}$, so the leading term of $e^{2A_s}V_{C,\chi\chi}$ is $\frac{\Phi'^2}{4} - \frac{\Phi'^2}{2}(-1 - f_{,\Phi}) + f_{,\Phi}\Phi'^2 = (\frac{3}{4} + \frac{3f_{,\Phi}}{2})\Phi'^2$. The Regge behavior of the spectral is determined by the leading IR behavior, the coefficient before Φ'^2 is proportional to the Regge slope. In order to be consistent with the experimental data, we need $\frac{3}{4} + \frac{3f_{,\Phi}}{2} \to 0$ in the IR region, so the leading term of $f_{,\Phi} = -\frac{1}{2}$ and $f(\Phi) \to -\frac{1}{2}\Phi$. Then we examine the IR behavior of the EOM of χ,

$$-\frac{\Phi^{'}}{2}e^{-\frac{\Phi}{2}} - \Phi^{'}e^{-\frac{\Phi}{2}} \propto e^{f(\Phi)}V_{c,\chi}(\chi) \tag{4.32}$$

Note that when $z \to \infty$, we have $\Phi^{'} \propto z \propto \sqrt{\Phi}$ and $\chi \to const, V_{c,\chi}(\chi) \to const$, then we can know that when $\Phi \to \infty$, $f(\Phi) = -\frac{1}{2}\Phi + \frac{1}{2}\log\Phi$. If we hope in the small Φ region, $e^{f(\Phi)} = 1$, a simplest choice is

$$f(\Phi) = -\frac{\Phi}{2} + \frac{\log(1+\Phi)}{2}, \tag{4.33}$$

which leads to the coupling between dilaton background field and the scalar field at leading order taking the form of

$$V_C(\chi,\Phi) \sim \chi^2\Phi^2. \tag{4.34}$$

For our numerical calculations, we take two sets of parameters in Table 6. The parameters in Mod I has a smaller chiral condensate, which gives a smaller pion decay constant,

n	f_0 Exp (MeV)	Mod I (MeV)	Mod II (MeV)
1	550^{+250}_{-150}	460	231
2	980 ± 10	1069	1064
3	1350 ± 150	1381	1395
4	1505 ± 6	1629	1632
5	1724 ± 7	1845	1846
6	1992 ± 16	2038	2039
7	2103 ± 8	221	2215
8	2314 ± 25	2376	2376

Table 7. The experimental and predicted mass spectra for scalar mesons f_0.

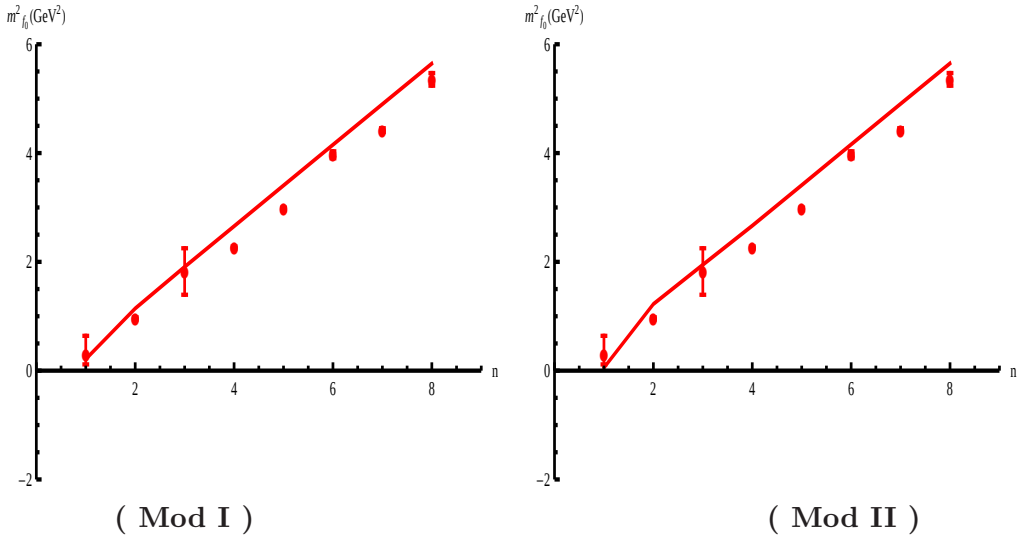

Figure 11. Scalar meson spectra $m^2_{f_0,n}$ as functions of n for Mod I and II defined in Table 6.

this will be discussed in Sec. 5. With two sets of parameters, the scalar spectra are shown in Table 7 and Fig. 11, and the corresponding wave-functions are shown in Fig. 12.

It is observed that in our graviton-dilaton-scalar system, the lowest scalar state has a positive mass, and the higher excitations behave a Regge line which agrees well with experimental data.

4.4.2 Pesudo-Scalar Sector

The terms of quadratic order in π and φ ($A^{\parallel}_{\mu} = \partial_\mu \varphi$) is

$$S^{(2)}_{\pi} = -\frac{N_f}{2N_c L^3}\int d^5x e^{-\Phi}\sqrt{g_s}(\chi^2 \partial_z \pi \partial^z \pi + \chi^2 \partial_\mu(\pi-\varphi)\partial^\mu(\pi-\varphi) + \frac{L^2}{g_5^2}\partial_z\partial_\mu\varphi\partial^z\partial^\mu\varphi). \tag{4.35}$$

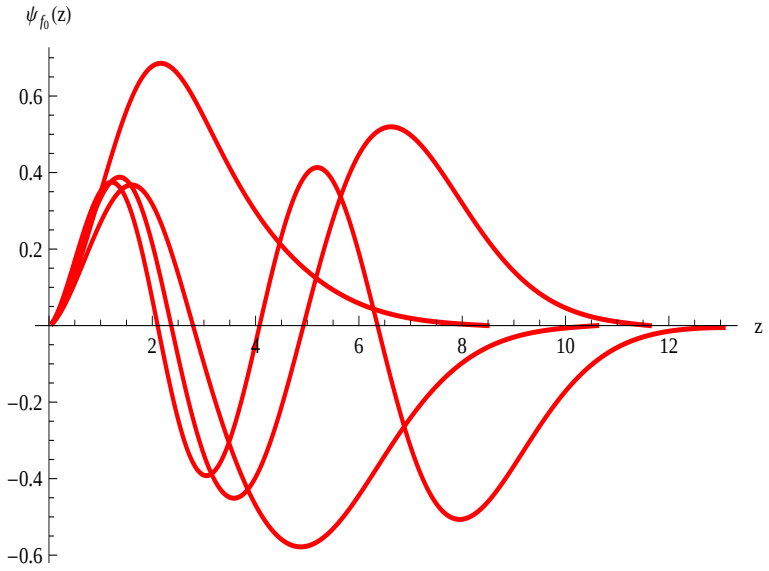

Figure 12. The scalar wave function $\psi_{f_0,n}(z)$ as function of z with $G_5 = \frac{3L^3}{4}, m_q = 5\text{MeV}, \sigma = (218\text{MeV})^3$.

The equations of motion for the pesudoscalar π coupled with φ take the form of

$$\begin{aligned} -e^{-(3A_s-\Phi)}\partial_z(e^{3A_s-\Phi}\chi^2\partial_z)\pi + q^2\chi^2(\pi-\varphi) &= 0, \qquad (4.36)\\ -e^{-(A_s-\Phi)}\partial_z(e^{A_s-\Phi}\partial_z)\varphi - g_5^2\chi^2 e^{2A_s}(\pi-\varphi) &= 0, \qquad (4.37)\end{aligned}$$

which can be written in the following form

$$\begin{aligned} -\ & \pi_n'' + V_{\pi,\varphi}\pi_n = m_n^2(\pi_n - e^{A_s}\chi\varphi_n),\\ -\ & \varphi_n'' + V_\varphi\varphi_n = g_5^2 e^{A_s}\chi(\pi_n - e^{A_s}\chi\varphi_n), \qquad (4.38)\end{aligned}$$

with the effective schrodinger potentials

$$\begin{aligned} V_{\pi,\varphi} &= \frac{3A_s'' - \Phi'' + 2\chi''/\chi - 2\chi'^2/\chi^2}{2} + \frac{(3A_s' - \Phi' + 2\chi'/\chi)^2}{4},\\ V_\varphi &= \frac{A_s'' - \Phi''}{2} + \frac{(A_s' - \Phi')^2}{4}. \qquad (4.39)\end{aligned}$$

With two sets of parameters in Table 6, the pseudoscalar spectra π are shown in Table 8 and Fig. 13, and the corresponding wave-functions are shown in Fig. 14. It is observed that in our graviton-dilaton-scalar system, the lowest pseudoscalar state has a mass around 140MeV, which can be regarded as the Nambu-Goldstone bosons due to the chiral symmetry breaking. The higher excitations behave a Regge line which agrees well with experimental data.

n	π Exp (MeV)	Mod I (MeV)	Mod II (MeV)
1	140	137	139.4
2	1300 ± 100	1498	1600
3	1816 ± 14	1865	1897
4	2070	2099	2116
5	2360	2287	2299

Table 8. The experimental and predicted mass spectra for pseudoscalar mesons π.

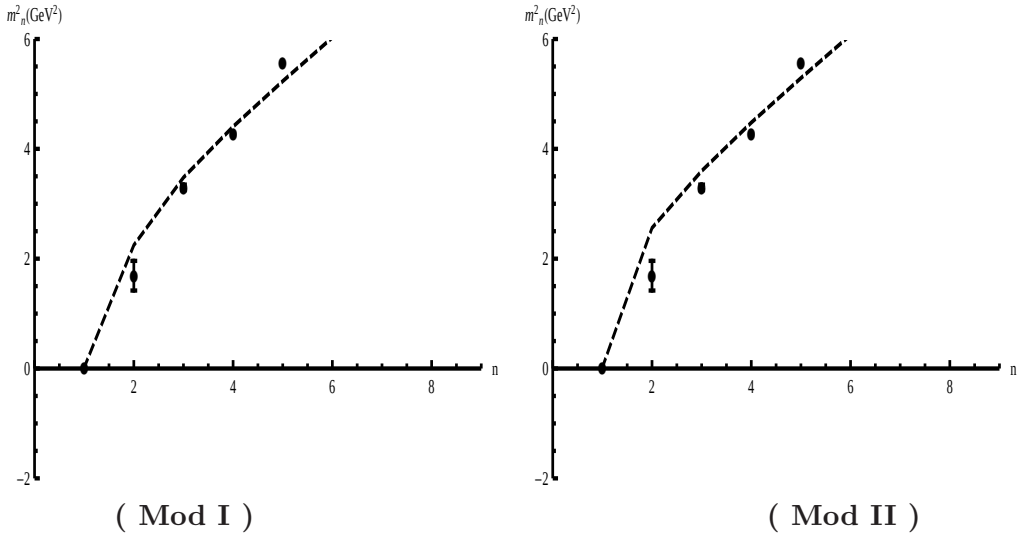

Figure 13. Pseudo-scalar spectra $m^2_{\pi,n}$ as function of n for Mod I and II defined in Table 6.

4.4.3 Vector sector

In the vector sector, the terms of quadratic order in $V^\perp$ are

$$S_V^{(2)} = -\frac{N_f}{2g_5^2 N_c L^3}\int d^5x e^{-\Phi} b_s^5 \left(\partial_z V_\mu^\perp \partial^z V^{\perp\mu} + \partial_\mu V_\nu^\perp \partial^\mu V^{\perp\nu}\right), \tag{4.40}$$

The equations of motion of the vector mesons take the form of

$$-\rho_n^{''} + V_v \rho_n = m_n^2 \rho_n, \tag{4.41}$$

with the schrodinger like potential

$$V_v = \frac{A_s^{'} - \Phi^{'}}{2} + \frac{(A_s^{'} - \Phi^{'})^2}{4}. \tag{4.42}$$

With two sets of parameters in Table 6, vector spectra are shown in Table 9 and Fig. 15, and the corresponding wave-functions are shown in Fig. 16. It is observed that in our

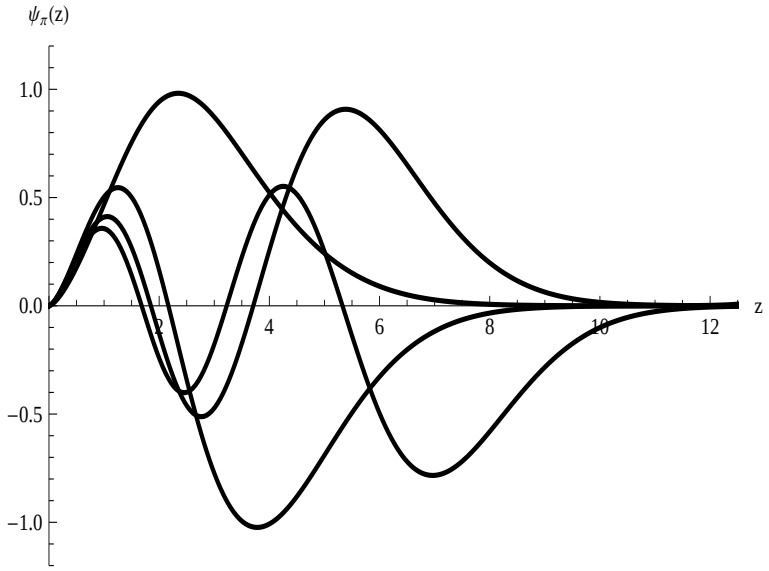

Figure 14. The pseudoscalar wave function $\psi_{\pi,n}(z)$ as function of z with $G_5 = \frac{3L^3}{4}, m_q = 5\text{MeV}, \sigma = (218\text{MeV})^3$.

n	ρ exp. (MeV)	Mod I. (MeV)	Mod II. (MeV)
1	775.5 ± 1	750	771
2	1282 ± 37	1139	1143
3	1465 ± 25	1428	1670
4	1720 ± 20	1667	1878
5	1909 ± 30	1876	2065
6	2149 ± 17	2063	2237
7	2265 ± 40	2235	2396

Table 9. The experimental and predicted mass spectra for vector mesons ρ.

graviton-dilaton-scalar system, the lowest vector state has a mass around $770MeV$, and the higher excitations behave a Regge line which agrees well with experimental data.

4.4.4 Axial Vector Sector

The terms of quadratic order in $A^\perp$ is

$$S_A^{(2)} = -\frac{N_f}{2g_5^2 N_c L^3}\int d^5x e^{-\Phi} b_s^5 \big(\partial_z A_\mu^\perp \partial^z A^{\perp\mu} + \partial_\mu A_\nu^\perp \partial^\mu A^{\perp\nu} + \frac{g_5^2\chi^2}{L^2} A_\mu^\perp A^{\perp\mu}\big). \quad (4.43)$$

The equations of motion of the axial-vector mesons take the form of:

$$-a_n^{''} + V_a a_n = m_n^2 a_n, \quad (4.44)$$

with the schrodinger potential for the axial vector as

$$V_a = \frac{A_s^{'} - \Phi^{'}}{2} + \frac{(A_s^{'} - \Phi^{'})^2}{4} + g_5^2 e^{2A_s}\chi^2. \quad (4.45)$$

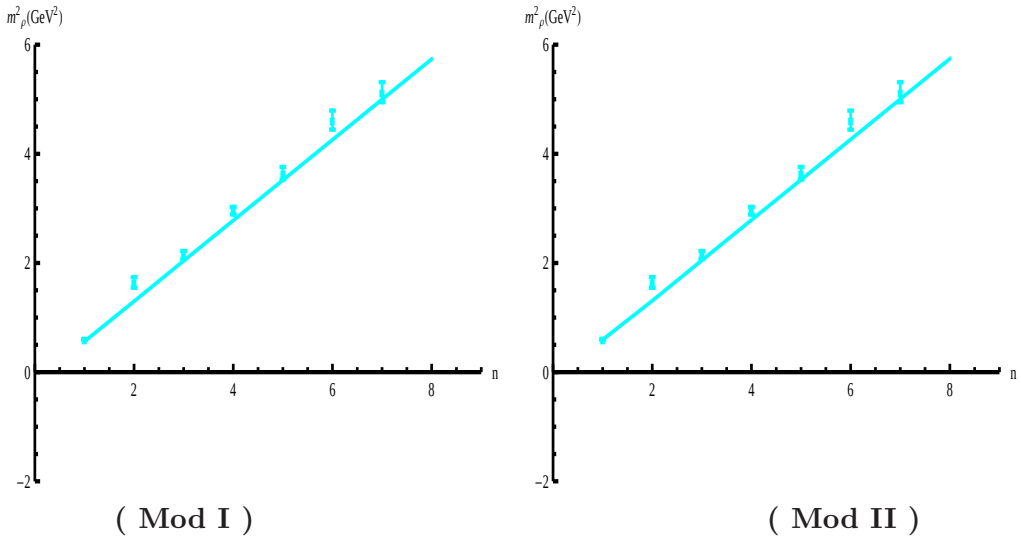

Figure 15. $m^2_{\rho,n}$ as function of n for Mod I and II defined in Table 6.

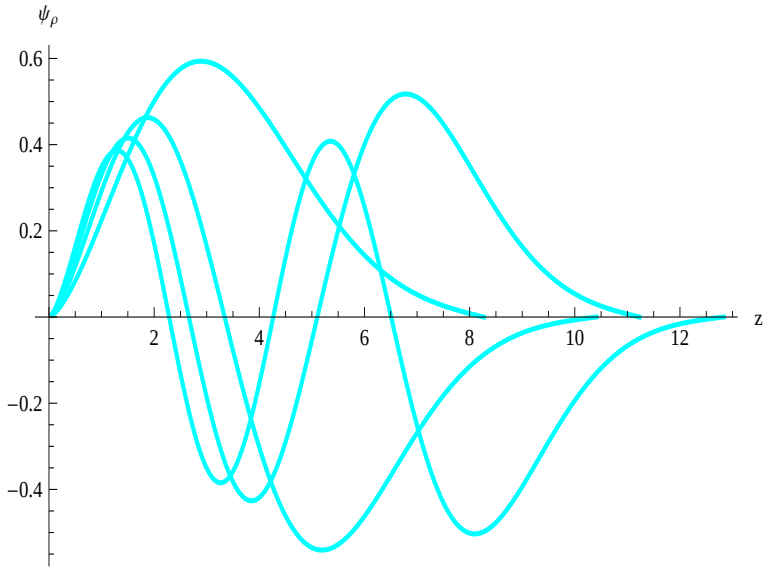

Figure 16. Pseudoscalar wavefunction $\psi_{\rho,n}(z)$ as function of z with $G_5 = \frac{3L^3}{4}, m_q = 5\text{MeV}, \sigma = (218\text{MeV})^3$.

As we can see that the difference between the schrodinger potentials for the axial vector Eq.(4.45) and vector Eq.(4.42) is only the extra term $g_5^2 e^{2A_s}\chi^2$ in Eq.(4.45). In the KKSS model, $g_5^2 e^{2A_s}\chi^2 \to 0$ when $z \to \infty$, therefore there is no splitting between vector and axial vector. Here in the graviton-dilaton-scalar system, $g_5^2 e^{2A_s}\chi^2 \to$ *constant* when $z \to \infty$,

n	a_1 Exp (MeV)	Mod I (MeV)	Mod II (MeV)
1	1230 ± 40	1219	1316
2	1647 ± 22	1691	1735
3	1930^{+30}_{-70}	1948	1969
4	2096 ± 122	2149	2163
5	2270^{+55}_{-40}	2326	2336

Table 10. The experimental and predicted mass spectra for axial vector mesons a_1.

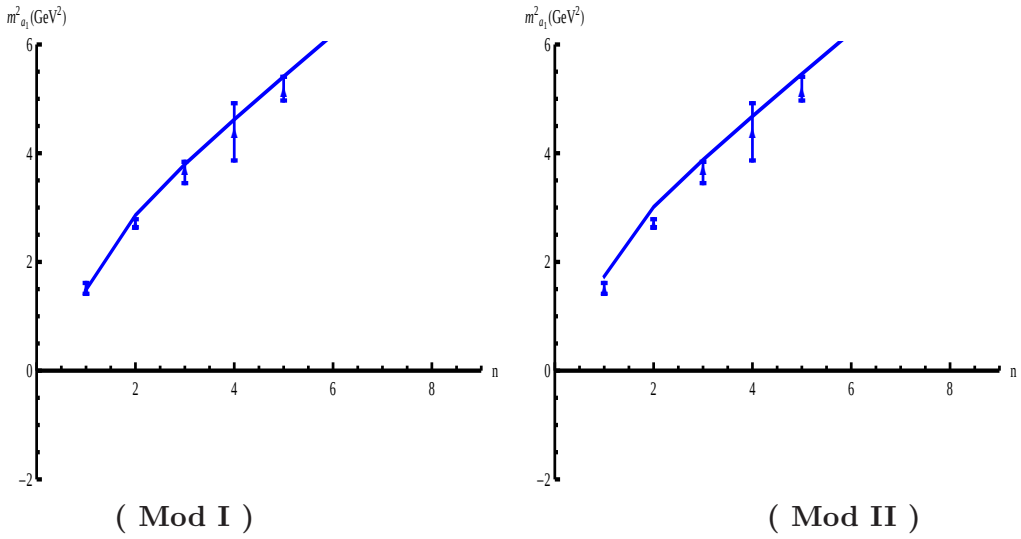

Figure 17. $m^2_{a_1,n}$ as functions of n for Mod I and II defined in Table 6.

which naturally induces the separation of the chiral partners.

With two sets of parameters in Table 6, vector spectra are shown in Table 10 and Fig. 17, and the corresponding wave-functions are shown in Fig. 18. It is observed that in our graviton-dilaton-scalar system, the lowest axial vector state has a mass around the experimental value $1230MeV$, and the higher excitations behave a Regge line which agrees well with experimental data.

4.5 Short summary

We summarize the meson spectra for scalar, pseudoscalar, vector and axial-vector in Fig. 19 for two sets of parameters. It is found that for both cases, the results are in very well agreement with experimental data. The ground state has the order of $m_\pi < m_{f_0} < m_\rho < m_{a_1}$, and the Regge slopes for scalar, pseudoscalar, vector and axial-vector meson at high excitations take the same value of $4\mu^2$.

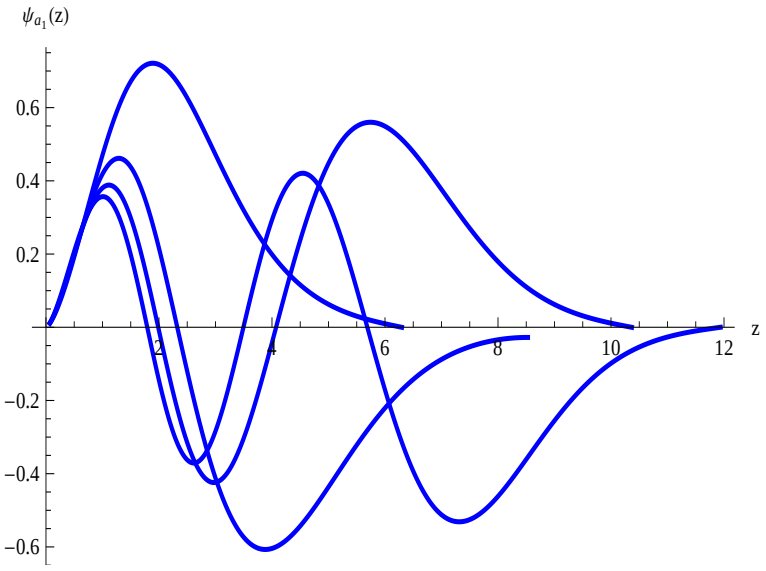

Figure 18. Axial-vector meson wave-function $\psi_{a_1,n}(z)$ as function of z with $G_5 = \frac{3L^3}{4}, m_q = 5\text{MeV}, \sigma = (218\ \text{MeV})^3$.

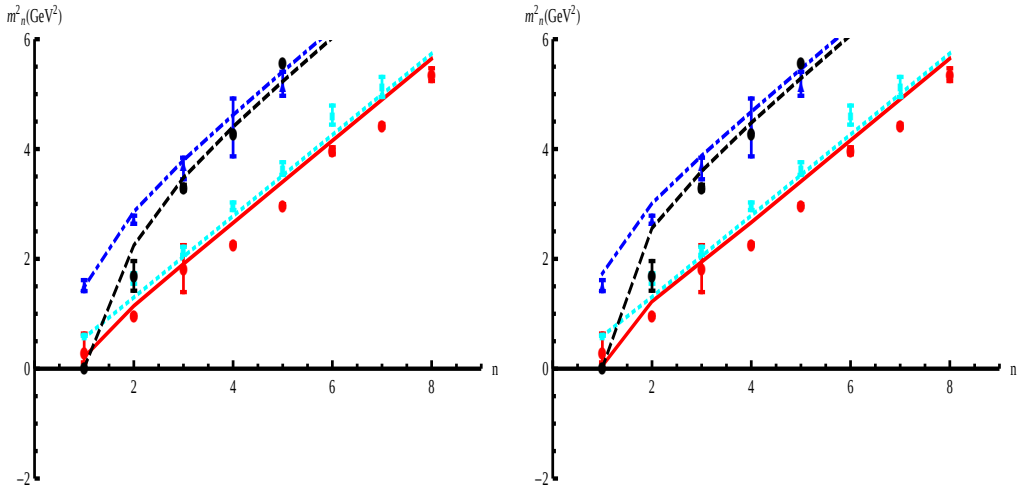

Figure 19. All meson spectra in the dynamical soft-wall model with two sets of parameters in Table 6 comparing with experimental data.

5 Decay constants, pion form factor and vector couplings

So far, within the above holography model we have studied one aspect of the static hadronic properties, the resonance masses. To further confirm this model, we have to check that whether it can reproduce reasonable behavior of other static and dynamic properties of hadronic physics, such as decay constants, vector couplings and form factors etc.

As in Ref.[21] (for more details see Ref. [102]), by studying the current-current correlation function and rewriting it as a summation over the normalizable wave functions, we can extract the decay constants $f_\pi, F_{\rho_n}, F_{a_1,n}$ as following,

$$f_\pi = -\frac{N_f}{g_5^2 N_c} e^{A_s-\Phi}\partial_z A(0,z)|_{z\to 0}, \tag{5.1}$$

$$F_{\rho_n}^2 = \frac{N_f}{g_5^2 N_c}(e^{A_s-\Phi}\partial_z V_n(z)|_{z\to 0})^2, \tag{5.2}$$

$$F_{a_1,n}^2 = \frac{N_f}{g_5^2 N_c}(e^{A_s-\Phi}\partial_z A_n(z)|_{z\to 0})^2. \tag{5.3}$$

Where $A(0,z), V_n(z), A_n(z)$ is the solution of equations

$$(-e^{-(A_s-\Phi)}\partial_z(e^{A_s-\Phi}\partial_z) + g5^2 e^{2A_s}\chi^2)A(0,z) = 0, \tag{5.4}$$

$$(-e^{-(A_s-\Phi)}\partial_z(e^{A_s-\Phi}\partial_z) - m_{\rho,n}^2)V_n(z) = 0, \tag{5.5}$$

$$(-e^{-(A_s-\Phi)}\partial_z(e^{A_s-\Phi}\partial_z) + g_5^2 e^{2A_s}\chi^2 - m_{a_1,n}^2)A_n(z) = 0, \tag{5.6}$$

with the boundary condition$A(0,0) = 1, \partial_z A(0,\infty) = 0$, $V_n(0) = 0, \partial_z V_n(\infty) = 0$,$A_n(0) = 0, \partial_z A_n(\infty) = 0$ and normalized as $\int dz e^{A_s-\Phi} V_m V_n = \int dz e^{A_s-\Phi} A_m A_n = \delta_{mn}$.

We can also extract the pion form factor from the three point correlator as [103–106]

$$f_\pi^2 F_\pi(Q^2) = \frac{N_f}{g_5^2 N_c}\int dz e^{A_s-\Phi} V(q^2,z)\{(\partial_z\varphi)^2 + g_5^2\chi^2 e^{2A_s}(\pi-\varphi)^2\}, \tag{5.7}$$

where$Q^2 = -q^2$, and $V(q^2,z), \pi(z), \varphi(z)$ is the solution of

$$(-e^{-(A_s-\Phi)}\partial_z(e^{A_s-\Phi}\partial_z) + q^2)V(q^2,z) = 0, \tag{5.8}$$

$$-e^{-(3A_s-\phi)}\partial_z(e^{3A_s-\phi}\chi^2\partial_z)\pi - m_{\pi,n}^2\chi^2(\pi-\varphi) = 0, \tag{5.9}$$

$$-e^{-(A_s-\phi)}\partial_z(e^{A_s-\phi}\partial_z)\varphi - g_5^2\chi^2 e^{2A_s}(\pi-\varphi) = 0, \tag{5.10}$$

with the boundary condition $V(q^2,0) = 1, \partial_z V(q^2,\infty) = 0, \pi(0) = 0, \partial_z\pi(\infty) = 0, \varphi(0) = 0, \varphi(\infty) = 0$ and normalized as

$$\frac{N_f}{g_5^2 N_c f_\pi^2}\int dz e^{A_s-\Phi}\{(\partial_z\varphi)^2 + g_5^2\chi^2 e^{2A_s}(\pi-\varphi)^2\} = 1. \tag{5.11}$$

To make sure that $F_\pi(0) = 1$ or equivalently we can write

$$F_\pi(Q^2) = \frac{\int dz e^{A_s-\Phi} V(q^2,z)\{(\partial_z\varphi)^2 + g_5^2\chi^2 e^{2A_s}(\pi-\varphi)^2\}}{\int dz e^{A_s-\Phi}\{(\partial_z\varphi)^2 + g_5^2\chi^2 e^{2A_s}(\pi-\varphi)^2\}}. \tag{5.12}$$

Decomposing F_π as in [103–106], we reach

$$F_\pi(Q^2) = \sum_n \frac{F_{\rho_n} g_{n\pi\pi}}{Q^2 + m_n^2}, \tag{5.13}$$

with

$$g_{n\pi\pi} = g_5\frac{\int dz e^{A_s-\Phi} V_n\{(\partial_z\varphi)^2 + g_5^2\chi^2 e^{2A_s}(\pi-\varphi)^2\}}{\int dz e^{A_s-\Phi}\{(\partial_z\varphi)^2 + g_5^2\chi^2 e^{2A_s}(\pi-\varphi)^2\}}. \tag{5.14}$$

	exp. (MeV)	Mod I. (MeV)	Mod II. (MeV)
f_π	92.4 ± 0.35	75	83.6
$F_\rho^{1/2}$	346.2 ± 1.4	277	282
$F_{a_1}^{1/2}$	433 ± 13	425	452
$g_{\rho\pi\pi}$	6.03 ± 0.07	3.59	3.14

Table 11. Decay constant in dynamical soft-wall model with two sets of parameters in Table 6.

	exp. (MeV)	Mod II.	KKSS	hard-wall	mod-soft	SWXY	GKK
f_π	92.4 ± 0.35	83.6	87.0	92.1	88.0	92.4	92.4
$F_\rho^{1/2}$	346.2 ± 1.4	282	261	329	325	—	—
$F_{a_1}^{1/2}$	433 ± 13	452	558	463	474	—	—
$g_{\rho\pi\pi}$	6.03 ± 0.07	3.14	3.33	4.48	4.63	3.51	2.89

Table 12. Table for decay constants and couplings from other models, the results in hard-wall,KKSS model stands, mod-soft are taken from [105, 106].

We would denote $g_{\rho\pi\pi} \equiv g_{0\pi\pi}$, i.e. putting the ρ meson ground state wave function $V_\rho \equiv V_0$ in the above equation.

The numerical results for the decay constant are shown in Table 11 and are compared with other models in Table 12.

We can see that both Mod I and Mod II give a smaller value of f_π than the experimental data, however we find that $m_q, \sigma, m_\pi, f_\pi$ in Mod I,II obeys the Gell-Mann-Oakes-Renner $2m_q\sigma = m_\pi^2 f_\pi^2$ with $\frac{m_\pi^2 f_\pi^2}{2m_q\sigma} - 1$ of order 0.1% within numerical errors and it checks the consistency of our model. The a_1 decay constants $F_\rho^{1/2}, F_{a_1}^{1/2}$ prediction is closer to the experimental data than other models, and both the prediction of the pion form factor are better than the original soft-wall model in Ref.[105, 106], while $F_\rho^{1/2}, g_{\rho\pi\pi}$ are a little too small.

The pion form factor is shown in Fig. 20, it is found that for parameters used in Mod I with a smaller chiral condensate, which corresponds to a smaller pion decay constant, the pion form factor matches the experimental better.

6 Discussion and summary

In this work, we construct a quenched dynamical holographic QCD (hQCD) model in the graviton-dilaton framework for the pure gluon system, and develop a dynamical hQCD model for the two flavor system in the graviton-dilaton-scalar framework by adding light flavors on the gluodynamical background. The dimension-2 dilaton background field takes the same form as that in the soft-wall model, i.e. $\Phi = \mu^2 z^2$, and its square Φ^2 can

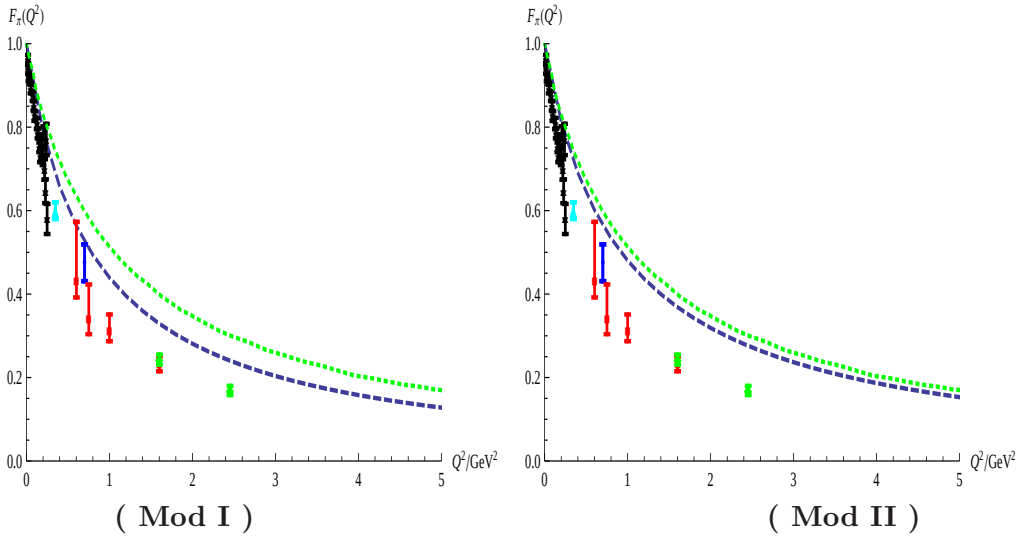

Figure 20. $F_\pi(Q^2)$ as function of Q^2 for Mod I and II defined in Table 6 and compared with experimental data.The blue dashed lines are the prediction in our model, and the green dotted line is the original soft-wall model results taken from Ref.[105, 106].

be identified as the dual field to the gauge invariant operator of the dimension-4 gluon condensate $< \mathrm{Tr}G^2 >$. The gluon condensate in the QCD vacuum breaks conformality and naturally induces a deformed warp factor, which can be self-consistently solved in the graviton-dilaton and graviton-dilaton-scalar framework.

In the quenched dynamical model, without introducing extra parameters but just self-consistently solving the deformed metric induced by the dilaton background field, we find that the scalar glueball spectra is in very well agreement with lattice data, while the soft-wall model with AdS_5 metric cannot accommodate both the ground state and the Regge slope for the scalar glueball spectra. We also give a necessary condition for the existence of linear quark potential from the metric structure, and we show that in the graviton-dilaton framework, a negative quadratic dilaton background field cannot produce the linear quark potential.

For two flavor system in the graviton-dilaton-scalar framework, the deformed metric is self-consistently solved by considering both the chiral condensate and gluon condensate in the vacuum, which are responsible for the chiral symmetry breaking and linear confinement, respectively. It is found that the mixing between the chiral condensate and gluon condensate is important in the dynamical hQCD model to produce the correct light flavor meson spectra.

The pion form factor and the vector couplings are also investigated in the dynamical hQCD model. In this part, the results in our model is not worse than the other models.

However, we emphasize that we have offered a systematic framework to describe the gluodynamics and chiral dynamics. The input in our model is basically the gluon condensate represented by μ^2, the chiral condensate σ, and a current quark mass m_q, which are the same as in the soft-wall model. Just solve the deformed warp factor self-consistently,

we can produce the glueball spectra, the linear heavy quark potential as well as light flavor meson spectra in very well agreement with lattice and experimental data.

Acknowledgement

This work is supported by the NSFC under Grant Nos. 11175251 and 11275213, DFG and NSFC (CRC 110), CAS key project KJCX2-EW-N01, K.C.Wong Education Foundation, and Youth Innovation Promotion Association of CAS.

References

[1] J. B. Kogut, "A Review of the Lattice Gauge Theory Approach to Quantum Chromodynamics," Rev. Mod. Phys. **55**, 775 (1983).

[2] R. Gupta, "Introduction to lattice QCD: Course," hep-lat/9807028.

[3] Z. Fodor and C. Hoelbling, "Light Hadron Masses from Lattice QCD," Rev. Mod. Phys. **84**, 449 (2012) [arXiv:1203.4789 [hep-lat]].

[4] J. C. R. Bloch, A. Cucchieri, K. Langfeld and T. Mendes, "Propagators and running coupling from SU(2) lattice gauge theory," Nucl. Phys. B **687**, 76 (2004) [hep-lat/0312036].

[5] R. Alkofer and L. von Smekal, "The Infrared behavior of QCD Green's functions: Confinement dynamical symmetry breaking, and hadrons as relativistic bound states," Phys. Rept. **353**, 281 (2001) [hep-ph/0007355].

[6] A. Bashir, L. Chang, I. C. Cloet, B. El-Bennich, Y. -X. Liu, C. D. Roberts and P. C. Tandy, "Collective perspective on advances in Dyson-Schwinger Equation QCD," Commun. Theor. Phys. **58**, 79 (2012) [arXiv:1201.3366 [nucl-th]].

[7] C. Wetterich, "Exact evolution equation for the effective potential," Phys. Lett. B **301**, 90 (1993).

[8] J. M. Pawlowski, "Aspects of the functional renormalisation group," Annals Phys. **322**, 2831 (2007) [hep-th/0512261].

[9] H. Gies, "Introduction to the functional RG and applications to gauge theories," Lect. Notes Phys. **852**, 287 (2012) [hep-ph/0611146].

[10] J. M. Maldacena, "The Large N limit of superconformal field theories and supergravity," Adv. Theor. Math. Phys. **2**, 231 (1998) [hep-th/9711200].

[11] S. S. Gubser, I. R. Klebanov and A. M. Polyakov, "Gauge theory correlators from noncritical string theory," Phys. Lett. B **428**, 105 (1998) [hep-th/9802109].

[12] E. Witten, "Anti-de Sitter space and holography," Adv. Theor. Math. Phys. **2**, 253 (1998) [hep-th/9802150].

[13] J. de Boer, E. P. Verlinde and H. L. Verlinde, "On the holographic renormalization group," JHEP **0008**, 003 (2000) [hep-th/9912012].

[14] K. Skenderis, "Lecture notes on holographic renormalization," Class. Quant. Grav. **19**, 5849 (2002) [hep-th/0209067].

[15] J. de Boer, "The Holographic renormalization group," Fortsch. Phys. **49**, 339 (2001) [hep-th/0101026].

[16] M. Li, "A Note on relation between holographic RG equation and Polchinski's RG equation," Nucl. Phys. B **579**, 525 (2000) [hep-th/0001193].

[17] I. Heemskerk and J. Polchinski, "Holographic and Wilsonian Renormalization Groups," JHEP **1106**, 031 (2011) [arXiv:1010.1264 [hep-th]].

[18] T. Faulkner, H. Liu and M. Rangamani, "Integrating out geometry: Holographic Wilsonian RG and the membrane paradigm," JHEP **1108**, 051 (2011) [arXiv:1010.4036 [hep-th]].

[19] V. Balasubramanian, M. Guica and A. Lawrence, "Holographic Interpretations of the Renormalization Group," JHEP **1301**, 115 (2013) [arXiv:1211.1729 [hep-th]].

[20] A. Adams, L. D. Carr, T. Schaefer, P. Steinberg and J. E. Thomas, "Strongly Correlated Quantum Fluids: Ultracold Quantum Gases, Quantum Chromodynamic Plasmas, and Holographic Duality," New J. Phys. **14**, 115009 (2012) [arXiv:1205.5180 [hep-th]].

[21] J. Erlich, E. Katz, D. T. Son and M. A. Stephanov, Phys. Rev. Lett. **95**, 261602 (2005); [22]

[22] A. Karch, E. Katz, D. T. Son and M. A. Stephanov, Phys. Rev. D **74** (2006) 015005.

[23] T. Sakai and S. Sugimoto, Prog. Theor. Phys. **113**, 843 (2005); Prog. Theor. Phys. **114**, 1083 (2006); G. F. de Teramond and S. J. Brodsky, Phys. Rev. Lett. **94**, 201601 (2005);L. Da Rold and A. Pomarol, Nucl. Phys. B **721**, 79 (2005);K. Ghoroku, N. Maru, M. Tachibana and M. Yahiro, Phys. Lett. B **633**, 602 (2006); O. Andreev, V.I. Zakharov, arXiv:hep-ph/0703010; Phys. Rev. D **74**, 025023 (2006); M. Kruczenski, L. A. P. Zayas, J. Sonnenschein and D. Vaman, JHEP **06**, 046 (2005); S. Kuperstein and J. Sonnenschein, JHEP**11**, 026 (2004). H. Forkel, M. Beyer and T. Frederico, JHEP **0707**, 077 (2007);

[24] Deog Ki Hong, Takeo Inami, and Ho-Ung Yee, Phys. Lett. B646:165-171, 2007; Kanabu Nawa, Hideo Suganuma, and Toru Kojo, Phys.Rev.D75:086003, 2007; Deog Ki Hong, Mannque Rho, Ho-Ung Yee, and Piljin Yi, Phys.Rev.D76:061901, 2007.

[25] C. Csaki, H. Ooguri, Y. Oz and J. Terning, JHEP **9901** (1999) 017. R. de Mello Koch, A. Jevicki, M. Mihailescu and J. P. Nunes, Phys. Rev. D **58** (1998) 105009; M. Zyskin, Phys. Lett. B **439** (1998) 373; J. A. Minahan, JHEP **9901** (1999) 020; C. Csaki, Y. Oz, J. Russo and J. Terning, Phys. Rev. D **59** (1999) 065012. R. C. Brower, S. D. Mathur and C. I. Tan, Nucl. Phys. B **587** (2000) 249; R. Apreda, D. E. Crooks, N. J. Evans and M. Petrini, JHEP **0405** (2004) 065. H. Boschi-Filho and N. R. F. Braga, JHEP **0305** (2003) 009; H. Boschi-Filho and N. R. F. Braga, Eur. Phys. J. C **32** (2004) 529; H. Boschi-Filho, N. R. F. Braga and H. L. Carrion, Phys. Rev. D **73**, 047901 (2006); H. Forkel, Phys. Rev. D **78**, 025001 (2008); P. Colangelo, F. De Fazio, F. Jugeau and S. Nicotri, Phys. Lett. B **652**, 73 (2007).

[26] O. Aharony, S.S. Gubser, J. Maldacena, H. Ooguri, Y. Oz, *Large N Field Theories, String Theory and Gravity,* Phys.Rept. 323(2000) 183; O. Aharony, arXiv:hep-th/0212193; A. Zaffaroni, PoS **RTN2005**, 005 (2005); J. Erdmenger, N. Evans, I. Kirsch and E. Threlfall, Eur. Phys. J. A **35**, 81 (2008), [arXiv:0711.4467 [hep-th]].

[27] G. F. de Teramond and S. J. Brodsky, "Hadronic Form Factor Models and Spectroscopy Within the Gauge/Gravity Correspondence," arXiv:1203.4025 [hep-ph]. Y. Kim, I. J. Shin and T. Tsukioka, "Holographic QCD: Past, Present, and Future," arXiv:1205.4852 [hep-ph].

[28] Y. Nambu, "Quasiparticles and Gauge Invariance in the Theory of Superconductivity," Phys. Rev. **117**, 648-663 (1960).

[29] J. Greensite, "Center vortices, and other scenarios of quark confinement," Eur. Phys. J. ST **140**, 1 (2007).

[30] G. Veneziano, Nuovo Cim. A **57**, 190 (1968); P.D.B. Collins, *An Introduction to Regge Theory and High Energy Physics*, Cambridge Univ. Press, Cambridge (1975).

[31] C. Amsler *et al.* [Particle Data Group Collaboration], Phys. Lett. B **667** (2008) 1.

[32] E. Eichten, K. Gottfried, T. Kinoshita, K. D. Lane and T. M. Yan, Phys. Rev. D **21**, 203 (1980).

[33] M. Huang, S. He, , Q. -S. Yan and Y. Yang, Eur. Phys. J. C **66**, 187 (2010) [arXiv:0710.0988 [hep-ph]].

[34] P. Colangelo, F. De Fazio, F. Giannuzzi, F. Jugeau and S. Nicotri, "Light scalar mesons in the soft-wall model of AdS/QCD," Phys. Rev. D **78**, 055009 (2008) [arXiv:0807.1054 [hep-ph]].

[35] T. Gherghetta, J. I. Kapusta and T. M. Kelley, Phys. Rev. D **79** (2009) 076003;

[36] Y. -Q. Sui, Y. -L. Wu, Z. -F. Xie and Y. -B. Yang, Phys. Rev. D **81** (2010) 014024; Y. -Q. Sui, Y. -L. Wu and Y. -B. Yang, Phys. Rev. D **83** (2011) 065030.

[37] B. Batell and T. Gherghetta, "Dynamical Soft-Wall AdS/QCD," Phys. Rev. D **78**, 026002 (2008) [arXiv:0801.4383 [hep-ph]].

[38] T. M. Kelley, S. P. Bartz and J. I. Kapusta, Phys. Rev. D **83** (2011) 016002; J. I. Kapusta and T. Springer, Phys. Rev. D **81**, 086009 (2010); T. M. Kelley, arXiv:1108.0653 [hep-ph]. T. M. Kelley, arXiv:1107.0931 [hep-ph].

[39] S. S. Afonin, Int. J. Mod. Phys. A **26**, 3615 (2011).

[40] W. de Paula, T. Frederico, H. Forkel and M. Beyer, Phys. Rev. D **79**, 075019 (2009).

[41] S. J. Brodsky and G. F. de Teramond, Phys. Lett. B **582**, 211 (2004); T. Branz, T. Gutsche, V. E. Lyubovitskij, I. Schmidt and A. Vega, Phys. Rev. D **82**, 074022 (2010).

[42] J. M. Maldacena, Phys. Rev. Lett. **80** (1998) 4859.

[43] O. Andreev and V. I. Zakharov, Phys. Rev. D **74**, 025023 (2006).

[44] H. J. Pirner and B. Galow, Phys. Lett. B **679**, 51 (2009).

[45] S. He, M. Huang and Q. S. Yan, Phys. Rev. D **83**, 045034 (2011).

[46] F. Zuo, Phys. Rev. D **82**, 086011 (2010).

[47] G. F. de Teramond and S. J. Brodsky, arXiv:0909.3900 [hep-ph].

[48] T. Gutsche, V. E. Lyubovitskij, I. Schmidt and A. Vega, Phys. Rev. D **85**, 076003 (2012).

[49] A. Karch, E. Katz, D. T. Son and M. A. Stephanov, JHEP **1104**, 066 (2011).

[50] D. Li, M. Huang and Q. -S. Yan, "A dynamical holographic QCD model for chiral symmetry breaking and linear confinement," arXiv:1206.2824 [hep-th].

[51] C. Csaki and M. Reece, JHEP **0705**, 062 (2007).

[52] S. S. Gubser and A. Nellore, "Mimicking the QCD equation of state with a dual black hole," Phys. Rev. D **78**, 086007 (2008) [arXiv:0804.0434 [hep-th]].

[53] U. Gursoy and E. Kiritsis, "Exploring improved holographic theories for QCD: Part I," JHEP **0802** (2008) 032; [arXiv:0707.1324 [hep-th]]. U. Gursoy, E. Kiritsis and F. Nitti,

"Exploring improved holographic theories for QCD: Part II," JHEP **0802** (2008) 019.

[54] D. Li, S. He, M. Huang and Q. -S. Yan, "Thermodynamics of deformed AdS_5 model with a positive/negative quadratic correction in graviton-dilaton system," JHEP **1109** (2011) 041.

[55] M. A. Shifman, A. I. Vainshtein, V. I. Zakharov, Nucl. Phys. **B147**, 385-447 (1979); **B147**, 448-518 (1979).

[56] G. Boyd, J. Engels, F. Karsch, E. Laermann, C. Legeland, M. Lutgemeier, B. Petersson, Nucl. Phys. **B469**, 419-444 (1996). [hep-lat/9602007].

[57] T. Schafer, E. V. Shuryak, Rev. Mod. Phys. **70**, 323-426 (1998). [hep-ph/9610451].

[58] L. S. Celenza and C. M. Shakin, "Description Of The Gluon Condensate," Phys. Rev. D **34**, 1591 (1986).

[59] M. J. Lavelle, M. Schaden, Phys. Lett. **B208**, 297 (1988).

[60] M. Lavelle, M. Oleszczuk, Mod. Phys. Lett. **A7**, 3617-3630 (1992).

[61] F. V. Gubarev, L. Stodolsky, V. I. Zakharov, Phys. Rev. Lett. **86**, 2220-2222 (2001). [hep-ph/0010057].

[62] H. Verschelde, K. Knecht, K. Van Acoleyen, M. Vanderkelen, Phys. Lett. **B516**, 307-313 (2001). [hep-th/0105018].

[63] K. G. Chetyrkin, S. Narison, V. I. Zakharov, Nucl. Phys. **B550**, 353-374 (1999). [hep-ph/9811275].

[64] F. V. Gubarev, V. I. Zakharov, Phys. Lett. **B501**, 28-36 (2001). [hep-ph/0010096].

[65] K. I. Kondo, Phys. Lett. B **514**, 335 (2001) [arXiv:hep-th/0105299].

[66] A. A. Slavnov, Theor. Math. Phys. **143**, 489 (2005) [Teor. Mat. Fiz. **143**, 3 (2005)] [arXiv:hep-th/0407194].

[67] B. Blossier, P. .Boucaud, M. Brinet, F. De Soto, Z. Liu, V. Morenas, O. Pene and K. Petrov *et al.*, Phys. Rev. D **83**, 074506 (2011); B. Blossier, P. .Boucaud, M. Brinet, F. De Soto, X. Du, M. Gravina, Z. Liu and V. Morenas *et al.*, arXiv:1111.3023 [hep-lat].

[68] F. Xu and M. Huang, "Electric and magnetic screenings of gluons in a model with dimension-2 gluon condensate," Chin. Phys. C **37**, 014103 (2013) [arXiv:1111.5152 [hep-ph]].

[69] P. Boucaud, A. Le Yaouanc, J. P. Leroy, J. Micheli, O. Pene and J. Rodriguez-Quintero, "Testing Landau gauge OPE on the lattice with a condensate," Phys. Rev. D **63**, 114003 (2001) [arXiv:hep-ph/0101302].

[70] D. Dudal, H. Verschelde, J. A. Gracey, V. E. R. Lemes, M. S. Sarandy, R. F. Sobreiro, S. P. Sorella, "Dynamical gluon mass generation from ¡A**2 (mu)¿ in linear covariant gauges," JHEP **0401**, 044 (2004). [hep-th/0311194].

[71] D. Dudal, H. Verschelde, R. E. Browne, J. A. Gracey, "A Determination of A**2(mu) and the nonperturbative vacuum energy of Yang-Mills theory in the Landau gauge," Phys. Lett. **B562**, 87-96 (2003). [hep-th/0302128].

[72] E. Ruiz Arriola and W. Broniowski, "Dimension-two gluon condensate from large-N(c) Regge models," Phys. Rev. D **73**, 097502 (2006) [hep-ph/0603263].

[73] M. N. Chernodub, E. -M. Ilgenfritz, "Electric-magnetic asymmetry of the A**2 condensate and the phases of Yang-Mills theory," Phys. Rev. **D78**, 034036 (2008). [arXiv:0805.3714 [hep-lat]].

[74] D. Vercauteren, H. Verschelde, "The Asymmetry of the dimension 2 gluon condensate: The Finite temperature case," Phys. Rev. **D82**, 085026 (2010). [arXiv:1007.2789 [hep-th]].

[75] J. M. Cornwall, "Quark Confinement and Vortices in Massive Gauge Invariant QCD," Nucl. Phys. B **157**, 392 (1979).

[76] J. M. Cornwall and A. Soni, "Glueballs as Bound States of Massive Gluons," Phys. Lett. B **120**, 431 (1983).

[77] J. M. Cornwall and A. Soni, "Couplings Of Low Lying Glueballs To Light Quarks, Gluons, And Hadrons," Phys. Rev. D **29**, 1424 (1984).

[78] A. A. Migdal and M. A. Shifman, "Dilaton Effective Lagrangian in Gluodynamics," Phys. Lett. B **114**, 445 (1982).

[79] C. Rosenzweig, J. Schechter and C. G. Trahern,

[80] R. Dick, "Confinement from a massive scalar in QCD," Eur. Phys. J. C **6**, 701 (1999) [hep-ph/9803209].

[81] D. Kharzeev, E. Levin and K. Tuchin, "Classical gluodynamics in curved space-time and the soft pomeron," Phys. Lett. B **547**, 21 (2002) [hep-ph/0204274].

[82] D. Kharzeev, E. Levin and K. Tuchin, "Broken scale invariance, massless dilaton and confinement in QCD," JHEP **0906**, 055 (2009) [arXiv:0809.3794 [hep-ph]].

[83] M. Chabab, "On the implications of a dilaton in gauge theory," Int. J. Mod. Phys. A **22**, 5717 (2007) [arXiv:0709.1226 [hep-ph]].

[84] D. Binosi, PoS LC **2010**, 020 (2010); A. C. Aguilar, D. Binosi and J. Papavassiliou, Phys. Rev. D **78**, 025010 (2008).

[85] A. Cucchieri and T. Mendes, PoS QCD **-TNT09**, 026 (2009); A. Cucchieri and T. Mendes, PoS LAT **2007**, 297 (2007); I. L. Bogolubsky, E. M. Ilgenfritz, M. Muller-Preussker and A. Sternbeck, PoS LAT **2007**, 290 (2007).

[86] D. Dudal, J. A. Gracey, S. P. Sorella, N. Vandersickel and H. Verschelde, Phys. Rev. D **78**, 065047 (2008).

[87] J. M. Cornwall, Phys. Rev. D **26**, 1453 (1982).

[88] K. -I. Kondo, "A nonperturbative construction of massive Yang-Mills fields without Higgs fields," Phys. Rev. D **87**, 025008 (2013) [arXiv:1208.3521 [hep-th]].

[89] M. Gell-Mann, Acta Phys. Austriaca Suppl. **9** (1972) 733. H. Fritzsch, M. Gell-Mann and H. Leutwyler, "Advantages Of The Color Octet Gluon Picture," Phys. Lett. B **47**, 365 (1973).

[90] V. Mathieu, N. Kochelev and V. Vento, arXiv:0810.4453 [hep-ph]; E. Klempt and A. Zaitsev, Phys. Rept. **454**, 1 (2007); C. Amsler and N. A. Tornqvist, Phys. Rept. **389**, 61 (2004).

[91] H. B. Meyer, "Glueball regge trajectories," hep-lat/0508002.

[92] B. Lucini and M. Teper, "SU(N) gauge theories in four-dimensions: Exploring the approach to N = infinity," JHEP **0106** (2001) 050 [hep-lat/0103027].

[93] C. J. Morningstar and M. J. Peardon, "The Glueball spectrum from an anisotropic lattice study," Phys. Rev. D **60** (1999) 034509 [hep-lat/9901004].

[94] Y. Chen, A. Alexandru, S. J. Dong, T. Draper, I. Horvath, F. X. Lee, K. F. Liu and N. Mathur *et al.*, "Glueball spectrum and matrix elements on anisotropic lattices," Phys.

Rev. D **73** (2006) 014516 [hep-lat/0510074].

[95] P. Colangelo, F. De Fazio, F. Jugeau and S. Nicotri, "On the light glueball spectrum in a holographic description of QCD," Phys. Lett. B **652**, 73 (2007) [hep-ph/0703316].

[96] H. Forkel, 'Holographic glueball structure," Phys. Rev. D **78**, 025001 (2008) [arXiv:0711.1179 [hep-ph]].

[97] H. Boschi-Filho, N. R. F. Braga, F. Jugeau and M. A. C. Torres, "Anomalous dimensions and scalar glueball spectroscopy in AdS/QCD," arXiv:1208.2291 [hep-th].

[98] K. Ghoroku, K. Kubo, T. Taminato and F. Toyoda, "Holographic Glueballs and Infrared Wall Driven by Dilaton," JHEP **1204**, 087 (2012) [arXiv:1111.7032 [hep-th]].

[99] S. J. Rey, S. Theisen and J. T. Yee, "Wilson-Polyakov loop at finite temperature in large N gauge theory and anti-de Sitter supergravity," Nucl. Phys. B **527**, 171 (1998) [arXiv:hep-th/9803135].

[100] L. Y. Glozman, "QCD symmetries in excited hadrons," arXiv:0710.0978 [hep-ph].

[101] M. Shifman and A. Vainshtein, "Highly Excited Mesons, Linear Regge Trajectories and the Pattern of the arXiv:0710.0863 [hep-ph];

[102] S. Hong, S. Yoon and M. J. Strassler, "On the couplings of vector mesons in AdS / QCD," JHEP **0604** (2006) 003 [hep-th/0409118].

[103] H. R. Grigoryan and A. V. Radyushkin, "Pion form-factor in chiral limit of hard-wall AdS/QCD model," Phys. Rev. D **76** (2007) 115007 [arXiv:0709.0500 [hep-ph]].

[104] H. R. Grigoryan and A. V. Radyushkin, "Form Factors and Wave Functions of Vector Mesons in Holographic QCD," Phys. Lett. B **650** (2007) 421 [hep-ph/0703069].

[105] H. J. Kwee and R. F. Lebed, "Pion form-factors in holographic QCD," JHEP **0801** (2008) 027 [arXiv:0708.4054 [hep-ph]].

[106] H. J. Kwee and R. F. Lebed, "Pion Form Factor in Improved Holographic QCD Backgrounds," Phys. Rev. D **77** (2008) 115007 [arXiv:0712.1811 [hep-ph]].